Geochemical Journal, Vol. 49, pp. 83 to 101, 2015 doi:10.2343/geochemj.2.0333

Oxygen isotopic heterogeneity of Pali Aike basaltic magmas from southern Patagonia as evidenced by oxygen isotope compositions of olivines

MI KYUNG CHOO,[1,2]* KYU HAN KIM,[2,3] JONG IK LEE,[1] MI JUNG LEE,[1] SUNG HI CHOI[4] and KYE-HUN PARK[5]

[1]Division of Polar Earth System Sciences, Korea Polar Research Institute (KOPRI), Incheon 406-840, Korea
[2]Department of Science Education, Ewha Womans University, Seoul 120-750, Korea
[3]Korea Institute of Geoscience and Mineral Resources (KIGAM), Daejeon 305-350, Korea
[4]Department of Earth and Environmental Sciences, Chungnam National University, Deajeon 305-764, Korea
[5]Department of Earth Environmental Science, Pukyong National University, Busan 608-737, Korea

(*Received November 21, 2013; Accepted September 8, 2014*)

Oxygen isotope ratios were determined using laser fluorination methods on 15 olivines and seven matrix samples separated from the Pali Aike alkali basalt of southern Patagonia. The $\delta^{18}O$ values were measured in ranges of 4.23 to 5.23‰ and 4.64 to 5.26‰ for olivine and matrix, respectively. The $\delta^{18}O$ values of Pali Aike olivines are lower and have a wider range than those of normal upper mantle (5.0–5.4‰). We considered that the heterogeneity of the oxygen isotope compositions of Pali Aike olivine provides evidence of assimilation at a shallow level and the presence of recycled material.

The differences between olivine and matrix $\delta^{18}O$ values indicate that $\Delta^{18}O_{(melt\text{-}ol)}$ (0.14 to 0.50) was within equilibrium fractionation for some and in disequilibrium for most samples at magmatic temperature. Oxygen isotope compositions in disequilibrium indicate that the lower $\delta^{18}O$ for the melt is explained by interaction with low $\delta^{18}O$ hydrothermally altered rocks. The low $\delta^{18}O_{olivine}$ values for low forsterite (Fo) contents of Pali Aike lavas can be explained by the effect of shallow-level assimilation. The oxygen isotope values for the olivine of high-MgO (or high-Fo) compositions are thought to represent oxygen isotope variation in the mantle source region. The low and variable $\delta^{18}O$ signature of Pali Aike olivine can be explained by crustal recycling, such as a contribution from the hydrothermally altered oceanic crustal melt. These heterogeneous oxygen isotope compositions indicate that Pali Aike olivines require both assimilation at a shallow level and a component of the high-μ end-members (HIMU) mantle derived from recycled mantle lithologies in the form of pyroxenite or eclogite.

Keywords: oxygen isotope, laser fluorination, Pali Aike olivine, Patagonia, HIMU

INTRODUCTION

The radiogenic isotopic signatures of intraplate volcanic rocks have demonstrated the existence of chemical heterogeneities in the Earth's mantle, and many studies have attempted to identify the geological processes responsible for the development of these heterogeneities (Barker *et al.*, 1997; Ferrari, 2004; Timm *et al.*, 2009, 2010). Chemical and isotopic heterogeneity of the Earth's mantle may coexist in the form of isotopically depleted and enriched domains such as depleted Mid-Ocean Ridge Basalt (MORB) mantle (DMM), enriched mantle I (EMI), enriched mantle II (EMII), and high-μ end-members (HIMU) (Zindler and Hart, 1986). It is thought that mantle might be depleted and enriched to a variety of extents of compositional heterogeneity because of partial melting and crustal extraction and the recycling of oceanic lithosphere back into the convecting mantle (Hofmann and White, 1982). However, it is difficult to distinguish processes of lithospheric material recycling using only variations in radiogenic isotopes because other geologic processes such as mantle metasomatism and crustal contamination yield similar fractionations of parent-daughter pairs. Thus, it has recently been suggested that the use of oxygen isotope systems may overcome some of the underlying limitations of using only radiogenic isotopes as tracers of lithospheric material in recycling processes (Harmon and Hoefs, 1995; Eiler *et al.*, 1996, 1997; Widom and Farquhar, 2003).

The olivines of mantle xenoliths ($\delta^{18}O$ within 4.9–5.5‰, Mattey *et al.*, 1994; Tollan *et al.*, 2012), mid-ocean ridge (MORB; $\delta^{18}O$ within 5.0–5.4‰, Eiler, 2001), and oceanic island basalts (OIB) exhibit a narrow range of oxygen isotope composition. Crustal rocks and sedimentary rocks are characterized by oxygen isotope values

*Corresponding author (e-mail: mkchoo@ewhain.net)

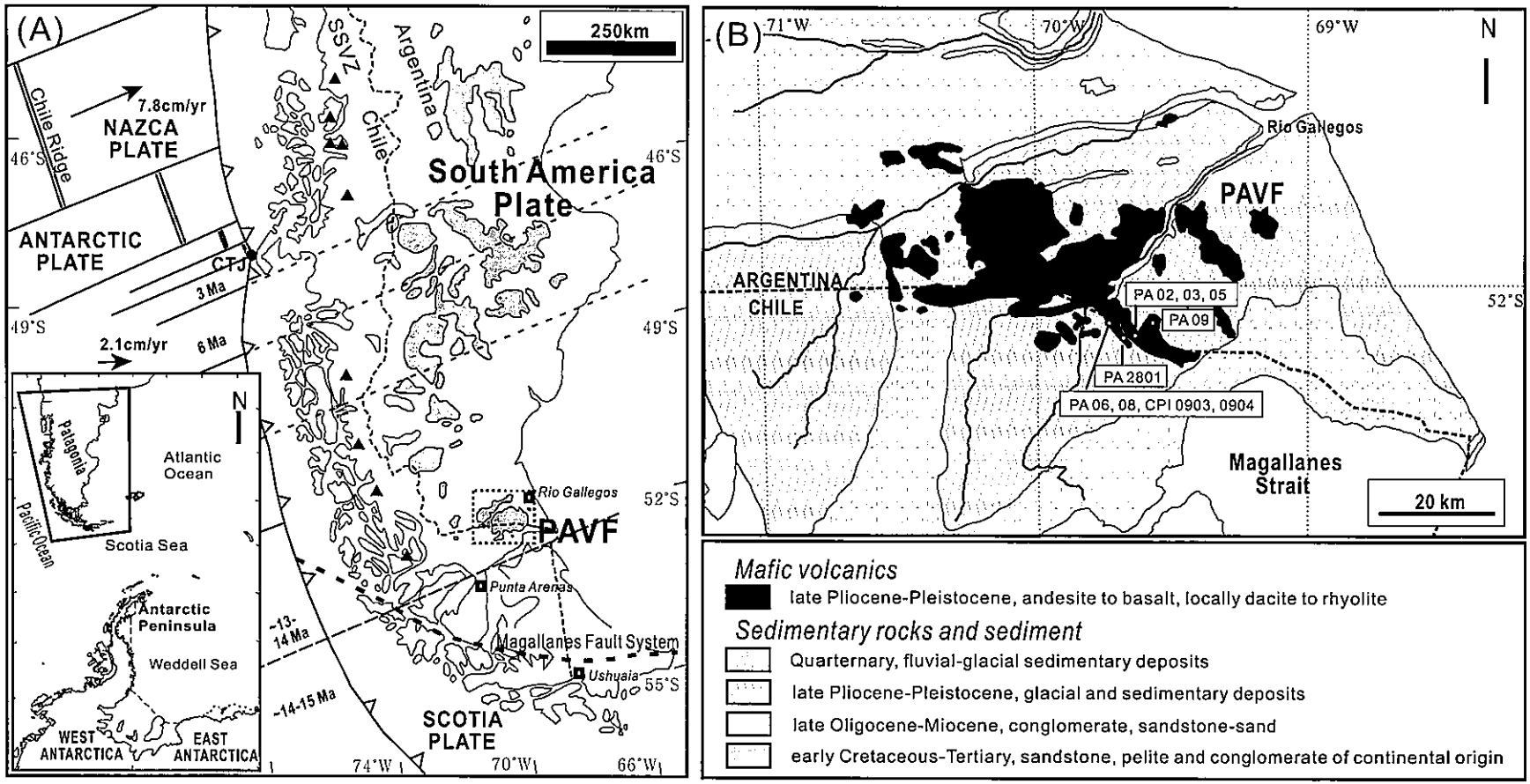

Fig. 1. (A) Regional tectonic setting of southern South America and the adjacent Pacific Ocean. The continuous lines in the Pacific Ocean are fracture zones of the oceanic Nazca and Antarctic plates. The Chile trench is indicated by a continuous line with triangles on the overriding plate, and the transcurrent margin between the Scotia and South American plates is shown by a dashed line. The Chile triple junction (CTJ) is indicated by the black circle. The main active volcanoes of the Austral volcanic zone (AVZ) and southern south volcanic zone (SSVZ) are represented by black triangles, and Cenozoic Patagonian plateau lavas are illustrated by the gray area. The two black arrows are convergence vectors of the Nazca and Antarctic plates relative to South America (Gripp and Gordon, 2002). Numbers indicate the collision ages of ridge segments with the Chile trench (Cande and Leslie, 1986). The inset is a geographic map of Patagonia and part of Antarctica modified from Pankhurst et al. (1998), D'Orazio et al. (2001), Ross et al. (2011), and Choo et al. (2012). (B) Geological map and sample locations for the Pali Aike volcanic field.

higher or lower than pristine mantle peridotites. Weathered and hydrothermally altered upper oceanic crust and pelagic sediments have $\delta^{18}O$ within 7–15‰ (Gregory and Taylor, 1981; Staudigel *et al.*, 1995) and 15–25‰ (Arthur *et al.*, 1983), respectively, which are higher than the mantle value. In contrast, $\delta^{18}O$ values of hydrothermally altered lower oceanic crust (0–6‰; Staudigel *et al.*, 1995) are lower than typical upper mantle peridotite. This excessive range of the variable oxygen isotopic values for mantle minerals shows the contributions of recycled components and crustal assimilation in the generation of magma (Widom and Farquhar, 2003).

The Pali Aike lavas are Cenozoic continental flood basalts near the southern tip of southern Patagonia. In general, continental flood basalts demonstrate a wide range of trace element and isotopic compositions, whereas some flood basalts clearly have chemical and isotopic signatures similar to those of oceanic basalts (e.g., Barker *et al.*, 2000; Gorring and Kay, 2001). Previous studies of Pali Aike lavas have focused mainly on the petrogenesis of products of mantle upwelling derived from asthenospheric melt using the slab-window model (Stern *et al.*, 1990; D'Orazio *et al.*, 2000; Choo *et al.*, 2012). Based on trace elements and Sr–Nd–Pb isotopic systematics of the Pali Aike lavas, Choo *et al.* (2012) proposed that (1) geochemical and isotopic characteristics of the Pali Aike lavas are broadly similar to those of Cenozoic HIMU basalts from the Antarctic Peninsula, West Antarctica, and New Zealand; (2) the petrogenesis of the Pali Aike basalts has a common history with the continental intraplate basalts of the HIMU magmatic megaprovince of the southwestern Pacific (e.g., Ferrar and Dixon, 1984; Weaver *et al.*, 1994; Finn *et al.*, 2005; Hoernle *et al.*, 2006a, b; Panter *et al.*, 2006; Sprung *et al.*, 2007; Timm *et al.*, 2009, 2010); and (3) the HIMU-like signature was produced by delamination (or detachment) of subcontinental lithospheric mantle of HIMU type at the time of breakup of Gondwana. In an oxygen isotope study of the aforementioned suggestion about Patagonian plateau basalts, the oxygen isotopes of Pali Aike olivine showed data for only two samples, and the lower $\delta^{18}O$ values were compared to those of arc basalts of southern Patagonia (Stern *et al.*, 1990). However, the oxygen isotope heterogeneity of the asthenospheric mantle of the Pali Aike lavas has not been discussed in detail.

In this study, we present new oxygen isotope data for olivine phenocrysts in alkali basalt from southern Patagonia and analyze the matrix to ascertain the equilibrium fractionation state between olivine and melt. The primary goals of our study are to better describe the oxygen isotope heterogeneity of mantle beneath Pali Aike and to evaluate the shallow level crustal assimilation for generation of continental flood basalts and the involvement of recycled components in the mantle.

Geological and Geochemical Setting

The Pali Aike volcanic field of southernmost South America is located on the border between Argentina and Chile in southern Patagonia (Fig. 1). The volcanic field is a ~4500-km^2 volcanic area located in a broader region consisting of parts of four lithospheric plates: the South American, Nazca, Antarctic, and Scotia plates (Fig. 1). Eastward subduction of the Nazca plate beneath southern South America occurred at a rate of ~8 cm/yr in the Cenozoic (Pardo-Casa and Molnar, 1987; DeMets *et al.*, 1994). The active Chile ridge separating the Nazca plate from the Antarctic plate collided with the Chile trench, and a triple ridge junction was created about 16 Ma (Breitsprecher and Thorkelson, 2009). The Cenozoic mafic magmatism in extra-Andean Patagonia south of the Chile triple junction is related to the opening of a slab window beneath South America associated with the subduction of the Chile ridge (Gorring *et al.*, 1997; D'Orazio *et al.*, 2000, 2001; Gorring and Kay, 2001).

The Pali Aike area (~52°S) is affiliated with the Pliocene–Quaternary Patagonian Plateau lava generated in back-arc position with respect to the Andes (Skewes and Stern, 1979). Isotopic ages (K–Ar and ^{40}Ar–^{39}Ar methods) for these basalts range from 3.78 to 0.17 Ma (Linares and Gonzalez, 1990; Singer *et al.*, 1997; Corbella, 1999; Lee *et al.*, 2000). Judging from several of the previously mentioned studies, these Pali Aike lavas are the youngest lavas from the final period of southern Patagonian magmatism. At the latitude of the Pali Aike volcanic field, the occurrence of primitive alkaline basalts, often bearing mantle xenoliths, about 200 km from the Austral volcanic zone (AVZ), is indicative of a deep fracture system that allowed rapid ascent of the magma to the surface (Choo *et al.*, 2012).

The petrography and geochemisty of the Pali Aike lavas have been studied by several authors (e.g., D'Orazio *et al.*, 2000; Lee *et al.*, 2000; Choo *et al.*, 2012). The Pali Aike basalts are porphyritic rocks having up to 20% phenocrysts containing forsteritic olivine with Cr-spinel inclusions, clinopyroxene, and plagioclase in an intergranular groundmass. Olivine phenocryst content in rocks in this study is within 10–15%. The reaction between olivine phenocrysts and the groundmass has not been observed in petrographic characteristics. Most of the studied basalts are very primitive, having MgO contents >9 wt.%, 147–400 ppm Ni and 194–436 ppm Cr, and Mg number [=100Mg/(Mg+Fe^{2+})] of 62 to 73 (Choo *et al.*, 2012). Sr and Nd isotopic compositions are more depleted ($^{87}Sr/^{86}Sr$ = 0.70327–0.70351, $^{143}Nd/^{144}Nd$ = 0.512882–0.512923; D'Orazio *et al.*, 2000; Choo *et al.*, 2012) than are those of Cenozoic mafic lavas from extra-Andean Patagonia ($^{87}Sr/^{86}Sr$ = 0.70355–0.70551, $^{143}Nd/^{144}Nd$ = 0.512614–0.512840; Gorring and Kay, 2001; Gorring *et*

al., 2003; D'Orazio *et al.*, 2005). The Pb isotopic composition ($^{206}Pb/^{204}Pb$ = 18.871–19.170; Choo *et al.*, 2012) has a HIMU-like signature, similar to that of the Antarctic Peninsula, West Antarctica, and New Zealand Cenozoic magmatism ($^{206}Pb/^{204}Pb$ = 19.01–20.93; Hart *et al.*, 1997; Panter *et al.*, 2000; Hoernle *et al.*, 2006a, b; Panter *et al.*, 2006; Sprung *et al.*, 2007; Nardini *et al.*, 2009; Timm *et al.*, 2009; McCoy-West *et al.*, 2010).

Analytical Techniques

Sample preparation and oxygen isotope analysis

We analyzed olivines and groundmass from 15 Pali Aike basaltic lavas. Olivine phenocrysts were handpicked from each crushed rock sample and examined with a binocular microscope to avoid inclusions, cracked or altered material, and irregular shapes. Separated olivine and matrix were 125–250 and 250–500-μm grain-size populations, respectively. The separated grains were cleaned ultrasonically in ultrapure water (18.3-MΩ MilliQ H_2O). To analyze oxygen isotopes for individual samples, approximately 1–2 mg samples composed of 1–10 individual crystals were prepared. For the typical characterization, from two to five replicates of each of the samples were analyzed. Oxygen isotope analyses were carried out using the laser fluorination technique of Kusakabe *et al.* (2004) at the Korea Polar Research Institute (KOPRI). The CO_2-laser BrF_5 fluorination system is detailed in Kusakabe *et al.* (2004), Kusakabe and Matsuhisa (2008), and Ahn *et al.* (2012). Oxygen was extracted in the form of O_2 from olivine and matrix samples using a laser fluorination system with a 10.6-μm CO_2 laser and bromine pentafluoride (BrF_5) oxidation. The reaction chamber with samples was evacuated and heated to 180°C for 12 h to remove surface contamination from the samples and atmospheric moisture in the reaction chamber. Then, the reaction chamber was prefluorinated with BrF_5 gas for at least 1 h at room temperature to remove any remaining atmospheric moisture of the samples or reaction chamber. After heating by the CO_2 laser, the extracted gas was purified through cryogenic traps at liquid nitrogen temperature, and the purified O_2 was collected in a 13× molecular sieve, also at liquid nitrogen temperature. The gas was analyzed with a mass spectrometer (PRISM, VG Isotech) with an online dual-inlet system connected to the purification line. To check the daily performance of the line for oxygen separation and the precision of oxygen values, standard materials were analyzed prior to and after treatment of the samples. The $\delta^{18}O$ values of the San Carlos olivine (SCO), Juan de Fuca ridge basalt glass (JFB), and NBS-28 quartz standards were measured to be 5.27 ± 0.04 (n = 21), 5.49 ± 0.02 (n = 148), and 9.18 ± 0.08 (n = 13), respectively (Ahn *et al.*, 2012). Analytical precision for this study can be judged from the mean values for JFB during the period of analysis (JFB = 5.49 ± 0.15‰, n = 16). Reported values of $\delta^{18}O$ are averages of duplicate or triplicate determinations with a precision of 0.1 to 0.2‰. The accuracy of the measured isotopic ratios may be assessed by comparison with the results of Ahn *et al.* (2012), Popova *et al.* (2013), and Warren *et al.* (2013). Replicate analyses of standards or unknown samples on the same day showed enhanced reproducibility (<±0.15‰, 2σ).

Mineral compositions

The chemical compositions of the olivines were analyzed using a JEOL JXA-8100 wavelength-dispersive electron microprobe with ZAF matrix correction at the Gyeungsang National University in Jinju, Korea. The instrument was operated with an accelerating voltage of 15 kV, beam current of 10 nA, beam diameter of ~1–3 μm, and counting time of 10 s. Based on repeated analyses of natural and synthetic standards, the relative analytical uncertainty for major and minor elements was <5%.

Major element, trace element, and radiogenic isotope analyses

Two samples (PA08 and PA09-1) were analyzed for whole-rock major and trace element concentrations. Major elements were analyzed by X-ray fluorescence (XRF) spectrometry using a Shimadzu XRF-1700 at the Cooperative Laboratory Center, Pukyong National University, Korea. Whole-rock trace element concentrations were determined by inductively coupled plasma mass spectrometry at the KOPRI in Incheon, Korea. Accuracy is estimated to be better than 5% for most trace elements. The results for major and trace element contents are presented in Table 1.

Seven samples (CPI0903, CPI0904-1, PA03, PA05-1, PA2801, PA09-1, and PA09-2) were analyzed for whole-rock Sr, Nd, and Pb isotope compositions. The chemical separation and mass spectrometry of Sr, Nd, and Pb for whole-rock isotopic analysis were performed at KOPRI. The column procedures have been described by Lee *et al.* (2011). Sr, Nd, and Pb isotope analyses were performed using a thermal ionization mass spectrometer (TIMS, Triton, Thermo Finnigan) equipped with nine adjustable Faraday cups. $^{87}Sr/^{86}Sr$ and $^{143}Nd/^{144}Nd$ ratios were corrected for instrumental mass fractionation by normalizing to $^{86}Sr/^{88}Sr$ = 0.1194 and $^{146}Nd/^{144}Nd$ = 0.7219, respectively. Replicate analyses of the NBS 987 and JNdi standards gave $^{87}Sr/^{86}Sr$ = 0.710260 ± 0.000004 (n = 20, 2σ) and $^{143}Nd/^{144}Nd$ = 0.512106 ± 0.000006 (n = 20, 2σ), respectively. Replicate analyses of the NBS 981 standard gave values of 36.486 ± 0.016, 15.422 ± 0.005, and 16.885 ± 0.005 for $^{208}Pb/^{204}Pb$, $^{207}Pb/^{204}Pb$, and $^{206}Pb/^{204}Pb$, respectively (mean, 2σ, n = 28). Total blanks averaged 50 pg for Sr and Nd and 300 pg for Pb. We consider that the

Table 1. Major and trace elements compositions for Pali Aike lavas

	Pali Aike	
Sample	PA08	PA09-1
Latitude (S)	52°04'52"	52°04'50"
Longitude (W)	69°46'93"	69°34'93"
Rock type	TeB	TB
Major elements (wt.%)		
SiO_2	44.65	45.55
Al_2O_3	11.52	10.57
TiO_2	3.80	3.12
Fe_2O_3	13.85	13.08
MnO	0.16	0.16
MgO	9.52	12.11
CaO	9.90	9.74
Na_2O	3.82	3.41
K_2O	2.09	1.67
P_2O_5	0.85	0.72
LOI*	0.01	0.00
Total	100.2	100.1
Mg# **	61.6	68.3
Trace elements (ppm)		
La	43.79	42.41
Ce	89.41	86.39
Pr	12.58	10.47
Nd	51.58	44.17
Sm	11.30	9.41
Eu	3.66	2.99
Gd	10.69	8.62
Tb	1.41	1.16
Dy	6.96	6.02
Ho	1.08	1.01
Er	2.70	2.49
Tm	0.27	0.31
Yb	1.67	1.77
Lu	0.19	0.23
Sc	19.73	
Th	4.66	4.33
U	1.21	1.25
Y	27.41	24.92
Hf	7.09	6.37
Mo	3.97	
Nb	65.71	54.48
Sn	2.56	
Ta	3.89	3.43
W	0.78	3.08
Zr	300	266
Ba	498	444
Pb	2.50	2.66
Cs	0.30	0.35
Li	7.70	7.20
Rb	30.66	26.87
Sr	936	736
Co	58.61	
Cu	52.56	
Ni	147	342

**LOI, Loss on Ignition.*
***Mg# = 100Mg/(Mg+Fe^{2+}), assuming Fe_2O_3/FeO = 0.15; TB, trachybasalt; TeB, tephrite basanite.*

Table 2. O–Sr–Nd–Pb isotope data for olivine phenocryst and matrix (O) and host basalt (Sr, Nd and Pb) from Pali Aike lavas

Sample name	Fo	1σ	MgO (wt.%)	$\delta^{18}O_{ol}$ (1)	$\delta^{18}O_{ol}$ (2)	$\delta^{18}O_{ol}$ (3)	$\delta^{18}O_{ol}$ (4)	$\delta^{18}O_{ol}$ (5)	Mean olivine	1σ	$\delta^{18}O_m$ (1)	$\delta^{18}O_m$ (2)	$\delta^{18}O_m$ (3)	$\delta^{18}O_m$ (4)	Mean matrix	1σ	$\Delta\delta^{18}O_{(ol-OH)}$	$^{87}Sr/^{86}Sr$	$^{143}Nd/^{144}Nd$	εNd	$^{208}Pb/^{204}Pb$	$^{207}Pb/^{204}Pb$	$^{206}Pb/^{204}Pb$
CPI0903	83.2	0.6	8.4	4.53	4.67	4.52	4.60		4.58	0.07	4.95	5.07			5.01	0.08	0.43	0.703370	0.512905	5.22	38.822	15.642	19.000
CPI0904-1	84.0	6.3	10.6	5.20	5.26				5.23	0.04								0.703288	0.512920	5.50	38.700	15.622	18.931
PA02-3	84.2	0.3	11.0	4.52	4.66				4.59	0.10	4.78	4.74			4.76	0.03	0.17	0.703433	0.512901	5.10	38.791	15.648	18.965
PA03	82.3	1.5	10.2	4.66	4.54	4.46	4.33		4.50	0.14	4.68	4.65	4.61	4.62	4.64	0.03	0.14	0.703441	0.512904	5.19	38.756	15.635	18.983
PA05-1	84.2	0.5	10.5	4.52	4.60	4.70			4.61	0.09								0.703399	0.512908	5.27	38.702	15.621	18.947
PA05-2	82.3	0.6	10.5	4.65	4.82	4.38	4.43		4.57	0.20	5.18	4.81	4.76		4.92	0.23	0.35	0.703404	0.512904	5.20	38.748	15.649	18.932
PA06	83.3	2.6	11.3	4.69	4.66	4.35			4.57	0.19	4.86				4.86	0.00	0.29	0.703272	0.512923	5.60	38.748	15.649	18.922
PA08	81.1	0.7	9.5	4.72	4.79				4.76	0.05	5.20	5.31			5.26	0.08	0.50	0.703302	0.512898	5.07	38.845	15.644	19.056
PA2801	86.3	2.6	13.7	4.73	4.98				4.86	0.18								0.703351	0.512917	5.44	38.687	15.626	18.981
PA09-1	86.4	1.5	12.1	4.78					4.78									0.703320	0.512823	3.62	38.948	15.664	19.193
PA09-2	85.2	1.2	12.1	4.89					4.89									0.703324	0.512877	4.66	38.903	15.656	19.179
PA09-3	85.8	3.1	12.0	4.59	4.62	4.78	4.79	4.81	4.72	0.10								0.703320	0.512883	4.80	38.905	15.663	19.168
PA09-4	85.5	0.4	11.1	4.19	4.21	4.30			4.23	0.06								0.703341	0.512887	4.90	38.864	15.643	19.158
PA09-05-1	86.8	3.7	11.7	4.69	4.61				4.65	0.06	4.81	4.90			4.86	0.06	0.21	0.703312	0.512882	4.80	38.909	15.659	19.170
PA09-05-2	85.7	0.3	11.6	4.48	4.52	4.68			4.56	0.11													

Data of Sr–Nd–Pb composition for PA02-3, PA05-2, PA09-3, PA09-4 and PA09-05-1 samples were analyzed by Choo et al. (2012).
εNd values were calculated using εNd = [($^{143}Nd/^{144}Nd)_{CHUR} - 1] \times 10^4$, where $(^{143}Nd/^{144}Nd)_{CHUR} = 0.512638$.

Table 3. Composition of olivine phenocrysts from Pali Aike lavas

	SiO_2	TiO_2	Al_2O_3	FeO^T	NiO	Cr_2O_3	MnO	MgO	CaO	Na_2O	K_2O	Total	Fo	Fo (mean)	1σ	X_{px}
CPI0903	39.94	0.02	0.04	15.74	0.29	—	0.19	43.94	0.24	0.01	—	100.4	83.27	83.23	0.63	0.64
	39.26	0.01	0.03	15.82	0.30	0.01	0.08	44.41	0.26	0.03	0.01	100.2	83.34			0.67
	39.55	—	0.01	16.61	0.27	0.02	0.28	43.13	0.27	0.02	0.04	100.2	82.24			0.67
	40.40	—	0.04	15.64	0.23	0.06	0.21	43.71	0.20	0.03	—	100.5	83.28			0.44
	39.47	0.02	0.04	15.10	0.28	0.05	0.20	44.48	0.29	0.02	—	99.9	84.00			0.58
CPI0904-1	38.36	—	0.02	20.96	0.15	0.06	0.32	40.34	0.38	—	—	100.6	77.43	82.41	6.32	0.38
	39.56	0.07	—	12.13	0.43	—	0.18	47.86	0.03	—	—	100.3	87.55			0.72
	41.77	—	0.04	9.61	0.34	0.03	0.12	48.54	0.07	0.04	0.00	100.5	90.01			0.28
	38.73	0.02	0.01	21.07	0.14	—	0.30	39.28	0.33	0.01	0.01	99.9	76.87			0.33
	41.00	0.02	0.07	11.28	0.43	0.02	0.17	47.08	0.21	0.01	0.01	100.3	88.16			0.64
PA02-3	39.51	0.02	—	15.05	0.18	0.03	0.24	45.01	0.31	0.05	—	100.4	84.21	84.21	0.33	0.20
	39.77	0.01	0.04	14.76	0.26	0.04	0.14	45.27	0.31	0.03	—	100.6	84.53			0.47
	39.21	0.04	0.04	15.42	0.19	0.05	0.15	45.01	0.25	0.02	—	100.4	83.88			0.26
PA03	39.10	0.02	0.04	17.65	0.24	0.07	0.27	42.51	0.35	0.03	—	100.3	81.11	82.33	1.48	0.61
	38.89	0.01	0.02	16.94	0.27	0.04	0.26	43.00	0.35	—	0.01	99.8	81.90			0.68
	40.29	—	0.06	15.19	0.26	0.00	0.19	44.65	0.32	0.01	—	101.0	83.98			0.51
PA05-1	40.13	—	0.04	15.37	0.20	0.06	0.22	44.01	0.27	0.02	—	100.3	83.62	84.17	0.47	0.30
	40.73	—	0.04	14.27	0.25	0.08	0.19	44.36	0.17	0.03	0.01	100.1	84.72			0.42
	40.77	0.00	0.05	14.77	0.22	0.05	0.19	44.65	0.26	—	—	101.0	84.35			0.33
	39.09	0.02	0.01	15.17	0.24	0.02	0.22	44.63	0.26	0.01	—	99.7	83.98			0.41
PA05-2	39.28	—	0.03	15.24	0.30	0.01	0.22	44.00	0.34	0.02	0.02	99.5	83.73	82.26	0.62	0.65
	40.34	—	0.06	14.75	0.20	0.04	0.20	44.30	0.25	0.01	—	100.2	84.26			0.25
	39.99	—	0.02	14.95	0.21	0.06	0.18	43.49	0.29	0.03	—	99.2	83.83			0.31
	40.31	—	0.07	15.74	0.20	0.06	0.27	42.51	0.31	0.04	0.01	99.5	82.80			0.34
PA06	39.20	—	0.07	21.67	0.19	—	0.32	38.83	0.40	0.03	0.05	100.8	76.16	77.54	2.55	0.66
	40.19	—	0.07	20.63	0.14	0.07	0.23	38.63	0.33	0.01	—	100.3	76.94			0.35
	37.66	—	0.04	21.60	0.16	—	0.32	39.29	0.36	0.04	0.01	99.5	76.43			0.48
	39.73	—	0.02	15.84	0.28	0.01	0.16	44.23	0.25	0.02	0.02	100.6	83.27			0.60
	38.55	—	0.03	21.02	0.14	0.02	0.28	39.94	0.34	0.00	—	100.3	77.21			0.33
	37.92	0.00	0.06	21.82	0.10	—	0.29	39.55	0.42	—	—	100.2	76.37			0.16
	38.91	0.03	0.01	21.66	0.13	—	0.26	39.36	0.34	0.01	—	100.7	76.41			0.31
PA08	38.90	0.01	0.05	18.16	0.06	0.01	0.25	41.84	0.27	0.03	0.04	99.6	80.42	81.06	0.74	—
	39.67	0.03	0.04	17.88	0.21	0.01	0.16	41.52	0.26	0.01	0.04	99.8	80.54			0.51
	39.68	0.02	0.08	17.87	0.14	0.03	0.27	42.27	0.25	0.04	0.01	100.7	80.83			0.20
	39.22	0.04	0.04	18.73	0.17	0.05	0.22	41.24	0.33	0.00	0.01	100.0	79.70			0.40
	40.86	0.01	0.02	16.93	0.16	0.03	0.21	42.34	0.28	—	0.01	100.9	81.68			0.25
	39.38	0.02	0.05	16.88	0.15	0.05	0.17	42.65	0.25	0.03	—	99.6	81.84			0.19
	39.69	0.10	0.01	17.45	0.19	0.03	0.18	42.60	0.27	0.03	—	100.5	81.32			0.37
	39.98	0.02	0.04	16.82	0.15	0.02	0.22	42.49	0.23	—	0.01	100.0	81.82			0.19
	39.32	0.05	0.03	17.38	0.19	0.01	0.21	42.71	0.29	—	—	100.2	81.42			0.39

procedural chemistry blanks were in all cases less than 0.5% of the sample amount and that the isotope ratios of blanks were not significantly different from those of analyzed samples. The results are given in Table 2.

RESULTS

Olivine composition

Chemical compositions of olivines are summarized in Table 3, which gives forsterite (Fo) contents and NiO, CaO, MnO, and Cr_2O_3 concentrations of olivine phenocrysts. Figure 2 shows the relationships between the contents of representative major oxides (NiO, CaO, MnO, and Cr_2O_3) and Fo contents of olivine phenocrysts. Fo contents of olivine range from 75 to 92 mol.% in the Pali Aike lavas. Positive correlations exist between Fo and NiO and between Fo and Cr_2O_3 and negative correlations between Fo and CaO and between Fo and MnO (Fig. 2). These linear correlations of major oxides versus forsterite indicate a trend of fractional crystallization.

Table 3. (continued)

	SiO_2	TiO_2	Al_2O_3	FeO^T	NiO	Cr_2O_3	MnO	MgO	CaO	Na_2O	K_2O	Total	Fo	Fo (mean)	1σ	X_{px}
PA2801	42.15	0.02	0.05	8.38	0.34	0.03	0.10	49.09	0.08	0.00	—	100.2	91.26	86.28	2.63	0.17
	40.51	0.11	0.03	14.51	0.36	—	0.13	44.30	0.09	0.05	—	100.1	84.48			0.80
	39.72	0.01	0.04	14.49	0.24	0.06	0.22	44.64	0.08	0.02	0.01	99.5	84.60			0.38
	40.24	0.01	0.03	9.90	0.34	0.00	0.10	48.75	0.05	0.02	0.01	99.4	89.77			0.29
	39.67	0.01	0.07	14.62	0.21	0.01	0.18	44.07	0.18	—	—	99.0	84.31			0.30
	41.08	0.01	0.05	13.28	0.30	0.01	0.17	45.76	0.11	0.00	0.02	100.8	86.00			0.49
	40.99	0.07	0.04	14.07	0.26	0.01	0.28	44.24	0.27	—	0.02	100.2	84.86			0.43
	40.60	0.02	0.03	14.34	0.22	0.05	0.14	44.71	0.23	—	—	100.3	84.75			0.31
	39.58	0.07	0.02	16.93	0.27	0.02	0.21	43.06	0.28	0.01	0.02	100.5	81.93			0.70
	40.88	—	0.04	11.27	0.41	0.01	0.14	47.16	0.12	—	0.02	100.0	88.18			0.59
	40.50	—	0.05	11.08	0.38	0.01	0.16	47.02	0.09	0.05	—	99.3	88.33			0.51
	40.68	0.07	0.04	9.97	0.42	0.02	0.11	48.60	0.04	0.03	—	100.0	89.68			0.48
	40.21	—	0.05	12.90	0.31	0.04	0.22	45.57	0.15	0.05	0.04	99.5	86.29			0.48
	39.67	0.02	0.06	15.40	0.26	—	0.15	43.94	0.34	—	0.02	99.8	83.57			0.51
	41.31	—	0.05	12.92	0.24	0.04	0.18	45.11	0.32	0.00	—	100.2	86.16			0.29
PA09-1	40.92	0.01	0.00	10.62	0.30	0.03	0.19	48.49	0.06	0.01	—	100.6	89.06	86.40	1.50	0.26
	40.38	0.02	0.06	13.26	0.22	0.01	0.16	45.80	0.25	0.02	—	100.2	86.03			0.24
	39.71	0.06	0.03	13.81	0.26	0.10	0.16	45.45	0.26	0.02	0.02	99.9	85.44			0.40
	40.64	—	0.03	13.58	0.24	0.03	0.14	45.16	0.28	—	0.02	100.1	85.57			0.34
	40.86	—	0.06	13.24	0.30	0.02	0.20	45.30	0.24	0.03	0.01	100.3	85.92			0.48
PA09-2	41.21	0.02	0.04	12.66	0.21	0.07	0.24	45.99	0.19	0.00	0.02	100.7	86.62	85.15	1.18	0.16
	39.76	0.02	0.06	13.94	0.31	0.11	0.13	45.98	0.27	0.01	—	100.6	85.46			0.54
	40.42	0.02	—	14.39	0.27	0.06	0.19	44.62	0.34	—	—	100.3	84.68			0.47
	38.90	0.02	0.02	15.34	0.27	0.03	0.21	44.66	0.33	0.03	0.04	99.8	83.84			0.54
PA09-3	40.25	0.04	0.04	14.44	0.24	0.07	0.26	45.36	0.28	0.01	0.01	101.0	84.85	85.78	3.07	0.35
	40.20	—	0.02	9.64	0.34	0.01	0.14	49.14	0.05	—	—	99.5	90.08			0.27
	39.98	0.02	0.03	13.16	0.27	0.08	0.19	45.42	0.27	0.02	0.00	99.4	86.02			0.38
	39.68	—	0.01	12.93	0.16	—	0.19	46.75	0.29	0.03	—	100.1	86.57			0.04
	40.00	0.01	0.03	12.76	0.30	0.10	0.20	46.31	0.28	0.00	0.03	100.0	86.61			0.44
	39.13	0.04	0.04	18.72	0.26	0.09	0.30	41.60	0.39	—	—	100.6	79.84			0.78
	40.36	0.02	0.04	12.78	0.29	0.02	0.17	46.08	0.17	0.04	0.01	100.0	86.53			0.40
PA09-4	41.33	—	0.04	13.75	0.10	0.03	0.19	44.83	0.24	0.02	—	100.5	85.32	85.54	0.36	—
	40.25	—	0.01	13.62	0.25	0.08	0.12	44.50	0.29	—	—	99.1	85.34			0.36
	40.93	—	0.04	13.12	0.33	0.01	0.15	45.07	0.18	—	—	99.8	85.96			0.59
PA09-05-1	41.89	—	0.04	9.14	0.43	—	0.12	48.87	0.01	0.01	—	100.5	90.51	86.75	3.70	0.41
	41.08	—	—	9.13	0.45	—	0.16	49.05	0.11	0.02	0.02	100.0	90.54			0.44
	41.73	—	—	13.63	0.27	0.07	0.17	44.71	0.21	—	—	100.8	85.40			0.43
	40.65	0.00	0.04	13.71	0.24	0.10	0.13	44.63	0.20	0.02	0.01	99.7	85.30			0.35
	40.14	—	0.06	16.53	0.23	0.03	0.23	42.32	0.35	—	—	99.9	82.03			0.50
PA09-05-2	40.38	0.05	0.03	13.18	0.38	0.08	0.15	45.81	0.21	0.01	—	100.3	86.11	85.69	0.34	0.71
	40.17	—	0.03	13.77	0.28	0.02	0.23	45.13	0.26	0.02	0.02	99.9	85.39			0.45
	41.44	0.02	0.05	13.43	0.18	—	0.20	44.92	0.27	0.01	0.01	100.5	85.64			0.14
	39.81	0.04	0.05	13.91	0.21	0.03	0.14	45.14	0.31	0.02	—	99.6	85.26			0.23
	40.68	0.01	0.05	13.33	0.34	0.04	0.14	44.80	0.29	0.04	0.02	99.7	85.69			0.64
	41.52	0.00	0.07	13.09	0.32	0.05	0.18	45.25	0.27	0.01	—	100.8	86.04			0.53

T: Total Fe as FeO.

X_{px}: weight fractionation of anticipated pyroxenite component calculated as Ni × FeO/MgO parameters using parameterization of Sobolev et al. (2008).

Oxygen isotopic compositions of olivines and basalts

Oxygen isotope analyses of 15 mineral and seven basalt fragments separated from 15 volcanic samples are presented in Table 2. The measured oxygen isotope values for olivine phenocryst and basalt fragments are 4.23–5.23‰ (mean $\delta^{18}O_{ol}$ = 4.67 ± 0.46‰ [2σ]) and 4.68–5.26‰ (mean $\delta^{18}O_{matrix}$ = 4.90 ± 0.40‰ [2σ]), respectively. These oxygen isotope values are lower than the

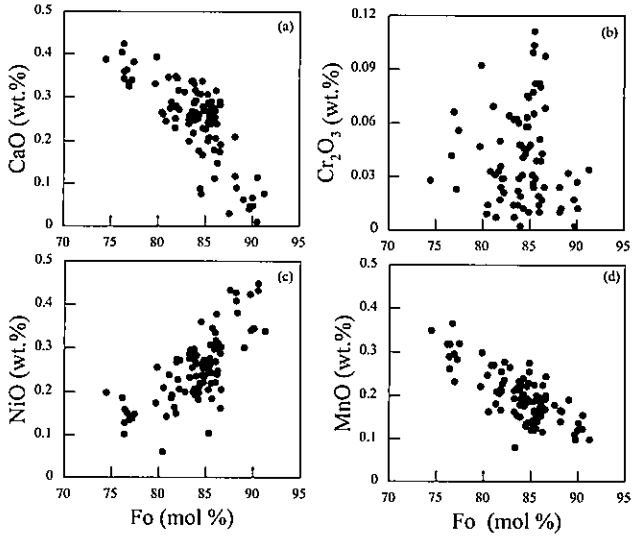

Fig. 2. Compositions of olivine phenocrysts from the Pali Aike lavas. The olivines are shown on plots of Fo content (mol.%) versus the element concentrations of (a) NiO, (b) CaO, (c) Cr_2O_3, and (d) MnO. Circles represent data for individual Pali Aike olivines.

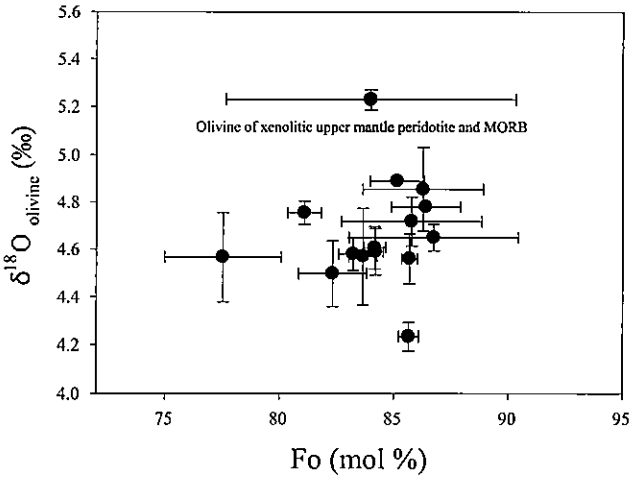

Fig. 3. Forsterite content (mol.%) versus oxygen isotope composition ($\delta^{18}O_{olivine}$‰) of Pali Aike olivines for each sample. The gray field indicates the $\delta^{18}O$ range of olivine from xenolith upper mantle peridotite and MORB sources (4.9–5.5‰; Mattey et al., 1994; Eiler et al., 1997). Circles represent data for Pali Aike olivines.

range of values observed in olivine separated from a wide variety of mantle peridotite xenoliths, largely from subcontinental lithospheric mantle (5.18 ± 0.28‰, n = 76; Mattey *et al.*, 1994) and mid-ocean ridge basalt (MORB, 5.16 ± 0.18‰, n = 6; Eiler *et al.*, 1997), and the range reported for fresh MORB glass (5.35 to 6.05‰; Ito *et al.*, 1987; Eiler *et al.*, 2000) (Fig. 3). The olivines of the Pali Aike lavas extend to more ^{18}O-depleted signatures. However, values of basalt fragments are similar to the lowest $\delta^{18}O$ values displayed by OIBs (Eiler *et al.*, 1997; Day *et al.*, 2009, 2010; Gurenko *et al.*, 2010), which represent the HIMU end-member (5.03 ± 0.22‰; n = 14). The relationship between $\delta^{18}O_{ol}$ values and Fo contents is plotted in Fig. 3. Most of the olivine crystals reveal a broad positive correlation between $\delta^{18}O$ values and Fo values.

Whole-rock Sr–Nd–Pb isotopes

The newly obtained Sr–Nd–Pb isotopic compositions for some Pali Aike basalts of this study are $^{87}Sr/^{86}Sr$ = 0.703288–0.703441, $^{143}Nd/^{144}Nd$ = 0.512823–0.512920, $^{206}Pb/^{204}Pb$ = 18.931–19.193, $^{207}Pb/^{204}Pb$ = 15.621–15.664, and $^{208}Pb/^{204}Pb$ = 38.687–38.948 (Table 2). These values are within the range of the data of Choo *et al.* (2012).

Discussion

Most of the measured $\delta^{18}O$ values for Pali Aike olivines are ~1‰ lower than average mantle values (5.2 ± 0.2‰). Exceptionally, the $\delta^{18}O$ value of one sample (CPI0903) is within the normal upper mantle range. The measured $\delta^{18}O$ values for Pali Aike olivines are in a broad range, whereas the whole-rock Sr–Nd–Pb isotopic signatures have limited variation. Subsequently, we discuss interlaboratory comparison of oxygen isotope values and the reasons for the variability of oxygen isotope composition in Pali Aike olivines.

Inter-laboratory composition of oxygen isotope values

Many early studies used the conventional method to measure the oxygen isotopic composition of refractory minerals (e.g., olivine, zircon, and garnet). Recently, laser fluorination techniques have been developed to measure very small amounts of the samples, ranging from one to two milligrams, and to demonstrate the relatively low level of oxygen background.

We present $\delta^{18}O$ data for the SCO, JFB, and NBS 28 quartz standards, commonly used for demonstrating interlaboratory comparability using both the conventional method and the laser fluorination technique, in Supplementary Table S1. The oxygen isotope values of the SCO standard suggested by Eiler *et al.* (1996, 2000) are 5.18–5.25‰ by CO_2 laser-BrF_5 analysis of whole grains, and these values are similar to our standard values (5.27 ± 0.04, n = 21; Ahn *et al.*, 2012).

Previous oxygen isotope data (Stern *et al.*, 1990) for olivines from the Pali Aike basalt are limited to two values, 5.1 and 5.5‰. These data were obtained by conventional analysis using BrF_5 on a MAT 251 mass spectrometer designed by Kyser (1990). Our oxygen data show mainly low $\delta^{18}O$ values, but some of our data are

within the values of Stern *et al.* (1990). The oxygen values of this study represent from two to five replicate analyses. Stern *et al.* (1990) suggested an oxygen isotopic composition of 9.6‰ as the standard value of NBS-28 quartz by conventional analysis using BrF_5. This standard value of oxygen isotopes has been analyzed within a wide range of approximately 0.2‰ by standardization and analytical methods from the suggestion of Stern *et al.* (1990; Table S1). The standard value of $\delta^{18}O$ of NBS-28 quartz has been found to be 9.18–10.0‰ by both conventional and laser fluorination methods (Table S1). According to Ahn *et al.* (2012), the oxygen standard value of NBS-28 analyzed at KOPRI was 9.18 ± 0.08‰ (n = 13), which is the same as the value 9.18 ± 0.07‰ (n = 20) reported by Kusakabe and Matsuhisa (2008) using the laser fluorination method and close to the 9.23 ± 0.05‰ reported by Clayton and Mayeda (1983) and 9.22 ± 0.14‰ by Ito and Clayton (1983) using the conventional method (Table S1). The variety of measurements of oxygen isotopes reveals analytical bias and inter-laboratory discrepancies. Kusakabe and Matsuhisa (2008) suggested that the VSMOW-SLAP scaling method (Coplen, 1995) could minimize the systematic bias. Recently, Ahn *et al.* (2012) normalized the oxygen isotopic data by the same scaling factor to make SLAP measurements by matching with the recommended value (Coplen, 1995). As mentioned previously, our $\delta^{18}O$ data by laser fluorination are consistent with standard $\delta^{18}O$ data obtained by conventional fluorination techniques. However, analysis indicated that the oxygen isotopic values of the standard materials differed from interlaboratory values. Although our oxygen data for the olivine are lower than those of a previous study (Stern *et al.*, 1990), they are suitable for discussion of our oxygen values.

Oxygen isotope fractionation between olivine and melt

Olivine is one of the particularly important minerals for understanding the dynamics of the Earth's interior because olivine, which crystallizes early in the magmatic evolution of basaltic lavas and is often present in them as a major constituent, is the predominant phase in the upper mantle. Additionally, fresh groundmass is glassy matrix, which is similar to the composition of silicate melts at high temperature. Thus, to discuss oxygen isotope fractionation between olivine and melt, we can consider the groundmass to represent melt.

To check the equilibrium fractionation of oxygen isotopes between olivine and melt, we show the obtained values of $\delta^{18}O$ for olivine and basalt fragments from seven samples in Fig. 4. Kyser *et al.* (1981) and Chiba *et al.* (1989) suggested an experimental oxygen isotopic fractionation for mineral–basaltic liquid and mineral–mineral of mantle-derived mineral assemblages, for which $\Delta^{18}O_{melt\text{-}olivine}$ indicated equilibrium at magmatic temperatures and $\delta^{18}O$ values of phenocrysts reflected quenched magmatic conditions. The difference in the values of $\delta^{18}O$ between coexisting olivine and melt in our samples (average $\Delta^{18}O_{melt\text{-}ol}$ = 0.14–0.50) is within or outside equilibrium, assuming that fractionation values are calculated using the equation from Bindeman *et al.* (2004). Most matrices analyzed show no equilibrium with their olivine phenocrysts. In most samples, values of $\Delta^{18}O_{melt\text{-}olivine}$ are 0.3–0.4‰ lower than the equilibrium range. The result of disequilibrium between matrix and olivine $\delta^{18}O$ values in Pali Aike samples suggest that the lower $\delta^{18}O$ melt may be caused by interaction with low $\delta^{18}O$ hydrothermally altered rocks in Pali Aike, as was observed for Klyuchevskoy, Kamchatka (Auer *et al.*, 2009; Bindeman *et al.*, 2004), Iceland (Bindeman *et al.*, 2008), and Hawaii (Garcia *et al.*, 1998). Additionally, olivine has a relatively slow rate of oxygen diffusion such that oxygen isotopes in olivine phenocrysts offer advantages in maintaining mantle composition. In a following section, we describe the reasons for the heterogeneous $\delta^{18}O$ values of olivines in Pali Aike lavas.

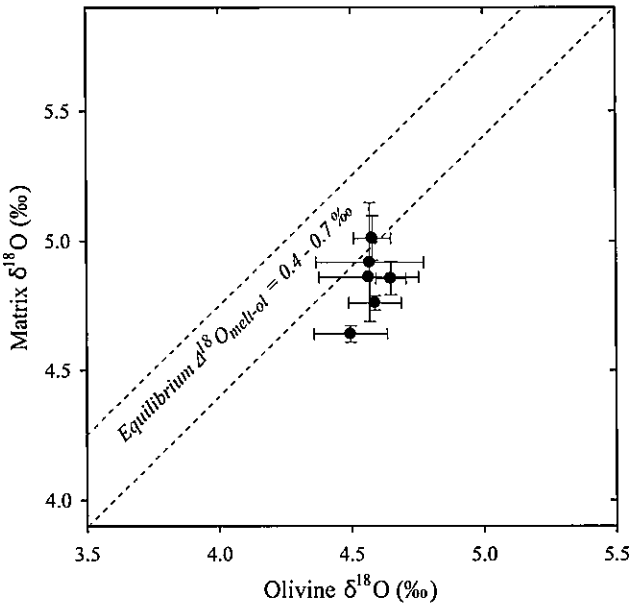

Fig. 4. Oxygen isotopic equilibrium between olivine and melt of Pali Aike lavas. The equilibrium field for melt-olivine isotopic fractionation was taken to be 0.4–0.7‰ (Bindeman et al., 2004). Symbols are the same as those in Fig. 2.

Source variations or shallow-level assimilation?

Erupted in southern Patagonia, the Pali Aike lavas are continental flood basalts. We can consider that the oxygen isotopic variability resulted from source variation or from shallow-level contamination (or assimilation). The oxygen isotope variability of approximately 1‰ in olivine

separated from the Pali Aike lavas is extended to low $\delta^{18}O$ values relative to mantle peridotite olivine. The lower values of some of the $\delta^{18}O$ could result from the assimilation of continental lithosphere and from the isotopic exchange of several minerals with shallow local meteoric water. The lithospheric mantle beneath Pali Aike is characterized as MORB type (5.2–6.0‰ for the $\delta^{18}O$ and 0.70264–0.70431 for the $^{87}Sr/^{86}Sr$ of mantle xenoliths; Stern *et al.*, 1999). The assimilation of the lithospheric mantle beneath Pali Aike is hard to resolve with all of the Pali Aike data. This is not supported by the radiogenic and trace element compositions of whole rocks in Pali Aike due to the requirement that a large amount of lithospheric mantle be assimilated.

Hydrothermal fluids around igneous plutons penetrated into the permeable upper crust. Exchange of oxygen and hydrogen isotopes of igneous rocks in the current of meteoric water can be generated by interaction with the hydrothermal fluid (Taylor and Epstein, 1962; Taylor, 1968; Sheppard and Taylor, 1974). Due to the lower $^{18}O/^{16}O$ ratio in the aqueous fluid, igneous rocks containing quartz, pyroxene, and feldspar represent low ^{18}O. The low values of the oxygen isotope ratio of these rocks generate the prominent volume by the occurrence of hydrothermal alteration in the upper crust. Those of mineral phases influenced by meteoric water depend on the temperature of the infiltrated fluid, the retention of the hydrothermal system, and the water–rock ratio (Criss and Taylor, 1986).

To assess possible assimilation of hydrothermally altered crust, we focus on the relationship between $\delta^{18}O$ values of olivine and Fo compositions (Fig. 3). The scattered relationship between the larger Fo and $\delta^{18}O$ range suggests the likelihood of a heterogeneous source, inherited from oxygen values that range more widely than those of pristine mantle, and assimilation of hydrothermally altered materials. Consequently, high-Fo olivine contents crystallized from the basic magma have retained their original heterogeneous oxygen isotopic values, whereas low-Fo olivines crystallized from somewhat evolved magma have undergone more involvement of the low-oxygen isotopic components for magma ascent through the mantle lithosphere (Garcia *et al.*, 1998).

Evidence for olivine alteration, interactions between olivine phenocrysts and groundmass, and effects of crustal assimilation has not been observed in thin sections in this study of Pali Aike lavas. The values of $\delta^{18}O$ of this study were measured by bulk oxygen isotope analysis of olivine without spot analyses on parts of cores or reaction rims of the minerals. Thus, it is very difficult to distinguish accurately whether olivine phenocrysts were crystallized at a shallow depth or retained in hydrothermally altered materials during the magma eruption.

Research findings for meteoric water in the Pali Aike volcanic area have revealed that the isotopic composition of groundwater in this area is <–8‰ for $\delta^{18}O$ and <–70‰ for δD (Mayr *et al.*, 2007). Erupted in the Upper Pliocene, Pali Aike lavas were positioned in the subpolar region, and continents around this area were covered with glaciers at that time. The isotopic composition of meteoric water during the eruptions was lower than it is today. Therefore, the low $\delta^{18}O$ value of the olivine phenocrysts could require a smaller amount of fluid components at magmatic temperatures.

The diffusion of oxygen isotopes in olivine and melt occurs at mantle temperatures. Low oxygen isotopic heterogeneity of olivine phenocrysts from Pali Aike lavas allows estimation of magma residence time of the crystals at mantle depth and then constraint of the lifetime or time scale of a magmatic system. Diffusion depends on the temperature and the diffusion coefficient (D), which is governed by the Arrhenius equation ($D = D_0 \cdot \exp(-Q/RT)$, where D_0 is the preexponential factor (D at $1/T = 0$), Q is the activation energy, R is the gas constant, and T is the temperature (K). Magma residence time at magmatic temperature is calculated by the parameters using this equation. We can estimate diffusion distances and times from one important application of the diffusion data (Cole and Chakraborty, 2001) and the homogenization or equilibration rates within minerals. Such estimates may be calculated by using an approximate relation $x^2 \approx D \cdot t$, where x is the effective diffusion distance (m), D is the diffusion coefficient (m^2/s), and t is time (s). Herein, we regard olivine crystals as spheres and assume immediate equilibration at the crystal–liquid boundary. Using the olivine diffusion coefficient of ^{18}O ($D = 2.73 \times 10^{-16}$, Dohmen *et al.* (2002); 8.15×10^{-17}; Yurimoto *et al.* (1992)) measured at 1100–1500°C, we can estimate the time of equilibration for oxygen isotopes. Assuming about 0.3-mm mineral size for analyzed samples and mantle temperature (1200°C), it is estimated that timescales of 10–35 m.y. will be required to complete O isotope re-equilibration prior to eruption. Moreover, alkali basaltic magma rapidly ascends toward the surface. From the study of mantle xenoliths in Pali Aike lavas, the depth of origin for the xenoliths is 60–70 km (Stern *et al.*, 1999), and the ascent rate is 6 ± 3 m/s (Demouchy *et al.*, 2006). The xenoliths are denser than the host magma, and this ascent rate is a minimum for the host alkali basaltic magma (McCoy-West *et al.*, 2010). Thus, the olivines in the Pali Aike volcanic area could not have remained at shallow levels for a very long time.

The evidence for shallow-level assimilation is supported by the relationship between $\delta^{18}O$ of olivine and the whole-rock $^{87}Sr/^{86}Sr$ (Fig. 5). Decreasing $\delta^{18}O$ values for olivine are broadly correlated with increasing $^{87}Sr/^{86}Sr$ for the whole rock. It is thought that the patterns of $\delta^{18}O$ evolution and slightly increasing $^{87}Sr/^{86}Sr$ are asso-

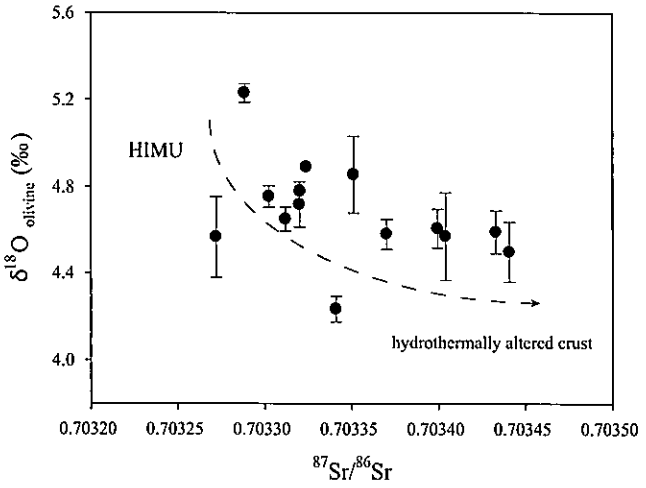

Fig. 5. Plot of whole-rock $^{87}Sr/^{86}Sr$ versus $\delta^{18}O$ olivines for Pali Aike lavas. The shaded region shows the mantle range of $\delta^{18}O$ olivine of HIMU OIB (4.6–5.2‰; Eiler et al., 1997; Day et al., 2009, 2010; Gurenko et al., 2010). Arrows on the dotted line indicate the effect of assimilation of hydrothermally altered crust. Symbols are the same as those in Fig. 2.

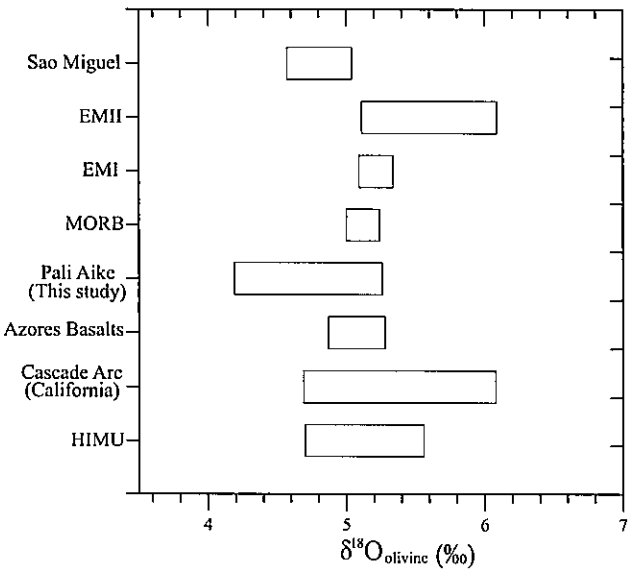

Fig. 6. Comparison of $\delta^{18}O$ values of olivine phenocrysts from the Pali Aike lavas with compiled $\delta^{18}O_{olivine}$ values of MORB (Eiler et al., 1997), HIMU OIB (Cook-Austral islands, Canary Islands, St. Helena, and Guadalupe; Eiler et al., 1997; Day et al., 2009, 2010; Gurenko et al., 2011), EMI (Eiler et al., 1997), EMII (Samoa; Workman et al., 2008), Sao Miguel (Widom and Farquhar, 2003), Azores basalts (Turner et al., 2007), and Cascade Arc (Martin et al., 2011).

ciated with assimilation of the hydrothermally altered crust. However, it is difficult to detect the process due to the small impact of crustal assimilation on geochemical data. In other words, the geochemical signatures of trace elements and radiogenic isotopes for basalts are relatively insensitive to crustal assimilation (Widom and Farquhar, 2003). In a previous study (Choo *et al.*, 2012), the ratios of Ce/Pb and Nb/U for the Pali Aike whole-rock samples were shown to be within the range of the MORB-OIB field (Hofmann *et al.*, 1986), together with the depleted $^{87}Sr/^{86}Sr$ and $^{143}Nd/^{144}Nd$ isotopic signatures of the Pali Aike lavas. It is difficult to measure the small amount of crustal assimilation using trace elements and radiogenic isotopic composition. Though the assimilation process during magma ascent has little effect on the chemical composition of the magma, crustal assimilation as a cause for the low $\delta^{18}O$ in low-forsterite olivines in the Pali Aike cannot be ruled out.

Recycled materials generating the heterogeneous $\Delta^{18}O$ isotopic compositions

The $\delta^{18}O$ of olivine in our samples ranged from 4.2 to 5.2‰, and O-isotope heterogeneity was outside analytical uncertainty (±0.15‰; 2σ). The $\delta^{18}O$ values of olivine for the Pali Aike lavas varied from the average of unmetasomatized mantle peridotite (5.2 ± 0.2‰; Mattey *et al.*, 1994) to lower (>4.2‰) values. Most olivines in the Pali Aike lavas had lower $\delta^{18}O$ values than those of upper mantle peridotites (5.0–5.4‰). From the scattered weak correlation between Fo and $\delta^{18}O$ shown in Fig. 3, it appears that the lower oxygen isotopic values for lower Fo contents could provide clues about assimilation processes; we focus on oxygen isotope variation for higher forsterite contents. Herein, oxygen isotope compositions for olivines of expected values (Fo > 85, MgO contents for whole rock >10 wt.%) for primitive magma range from 4.6 to 5.2‰ (by extrapolation). These values of oxygen isotopes of the Pali Aike lavas are different from those of normal asthenospheric mantle (5.0–5.4‰, Mattey *et al.*, 1994).

The $\delta^{18}O$ values of Pali Aike olivines show the range within pristine mantle olivines and HIMU OIB. To compare the oxygen isotopic composition of our samples with various mantle compositions obtained by laser fluorination, we have illustrated the HIMU type OIB (e.g., Cook-Austral Islands, Guadalupe, Canary Islands, and St. Helena; Eiler *et al.*, 1997; Day *et al.*, 2009, 2010; Gurenko *et al.*, 2011), EMII type OIB (Samoa; Workman *et al.*, 2008), Azores basalts (Turner *et al.*, 2007), and Cascade Arc basalt in California (Martin *et al.*, 2011) (Fig. 6). Pali Aike olivines are positioned as high MgO and plot within the range for HIMU-type OIB in the O–Sr–Pb isotope systematics (Figs. 5 and 8). It is thought that variation in $\delta^{18}O$ values in mantle-derived rocks are a signature of recycled materials at the sources. Lithospheric material can be recycled into the mantle and be involved in man-

tle sources. The recycled materials in the mantle can be summarized as three types: (i) altered upper basaltic oceanic crust, (ii) sediments, and (iii) hydrothermally altered lower oceanic crust (±lithosphere; Lassiter and Hauri, 1998; Schaefer *et al.*, 2002; Griffin *et al.*, 2003).

The recycling of subducted altered upper oceanic crust and pelagic sediments is a reasonable process for generating oxygen isotope heterogeneities in the mantle (Lassiter and Hauri, 1998). Crustal materials such as low-temperature altered rocks and sediments generally have variable and high ^{18}O values (Gregory and Taylor, 1981; Cocker *et al.*, 1982). Oxygen isotopic composition of the altered upper oceanic crust is approximately within the range 5–9‰ (Eiler, 2001). Moreover, the composition of oxygen isotopes in subducted pelagic sediments is strongly ^{18}O enriched (Eiler, 2001). Thus, mantle reservoirs into which subducted altered upper oceanic crust and sediments have been added have heavy oxygen isotope compositions, which is contrary to, and difficult to explain in light of, the depletion of ^{18}O in Pali Aike olivine.

The low and variable ^{18}O isotopic composition of the HIMU-like type mantle at Pali Aike could be explained by recycling of the lower oceanic crust (±lithosphere). Many studies of ophiolites have indicated that the fragment of oceanic crust has ^{18}O-enriched values in the upper oceanic crust and ^{18}O-depleted values in the lower oceanic crust (Geogory and Taylor, 1981; Cocker *et al.*, 1982). The diverse portions of the ophiolite including the hydrothermally altered lower crust (layer 3: gabbros and sheeted dikes) and the upper mantle ultramafic cumulate (harzburgite and dunite) have been shown to have depleted and variable $\delta^{18}O$ (Fig. 7). In general, gabbroic rock consists of various percentages of minerals including plagioclase, olivine, and pyroxene. Oxygen isotopic data for recent oceanic gabbro, ophiolitic gabbro, and transformed eclogite of Alpine gabbro are shown in Fig. 7. Metasomatism of peridotite by melts derived from recycled oceanic lithosphere produces pyroxenite or eclogite. Similar to this mechanism, descending basaltic and gabbroic parts of the oceanic lithosphere are transformed into the form of a silica-oversaturated eclogite at higher pressures (Hirschmann *et al.*, 2003; Kogiso *et al.*, 2003; Kogiso and Hirschmann, 2006). Roughly, pyroxenite dominated by layer-3 gabbros and sheeted dikes of oceanic crust lithologies have low $\delta^{18}O$ of 3–6‰ (an average of 4‰; Day *et al.*, 2009, 2010), but some gabbroic oceanic crust of the Samail ophiolite has an observed minimum $\delta^{18}O$ value of 1.7‰ (Thirlwall *et al.*, 2006). As noted in Fig. 7, the vein amphiboles of gabbroic rock in a lower crustal section in the Indian Ocean have low and varying $\delta^{18}O$ values of 1.2–5.4‰ (Stakes, 1991; Kempton *et al.*, 1991; Alt and Bach, 2006). Alternatively, oceanic crust is modified by subduction recycling, and these characteristics are shown in Alpine ophiolite generated by the dehydration processes of the transformation of gabbro to eclogite. The $\delta^{18}O$ values of these eclogitic rocks are 4.8 ± 0.9‰ (Fig. 7). To determine the contributions from recycled oceanic crust in the mantle beneath Pali Aike, we focused on the $\delta^{18}O$ values of Taitao ophiolite oceanic crust along the coast of Chile in southern Patagonia. Taitao ophiolite associated with the Chile ridge has been studied recently, in which its whole-rock $\delta^{18}O$ values for peridotite range from 2.5 to 5.0, whereas whole-rock $\delta^{18}O$ values for mafic rocks vary from 0.7 to 6.1 (Schulte *et al.*, 2009).

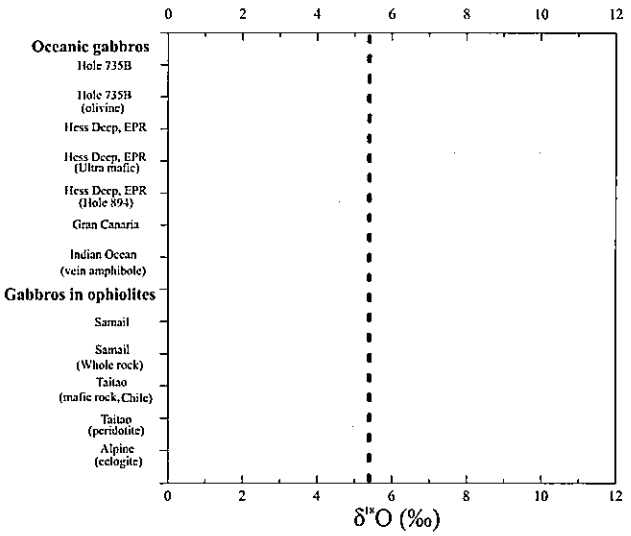

Fig. 7. Comparison of the $\delta^{18}O$ values of gabbros from contemporary oceanic crust and ophiolites. The dotted line at 5.2 ± 0.2‰ indicates the oxygen isotopic composition of olivine in unaltered MORB. Oceanic gabbros and gabbros in ophiolites are from Gregory and Taylor (1981), McCulloch et al. (1981), Kempton et al. (1991), Stakes (1991), Agrinier et al. (1995), Hart et al. (1999), Lecuyer and Reynard (1996), Barnicoat and Cartwright (1997), Hansteen and Troll (2003), Muehlenbachs et al. (2004), and Schulte et al. (2009).

As mentioned above, mantle characteristics with variable and low $\delta^{18}O$ values of Pali Aike olivine could have been affected by hydrothermally altered lower oceanic crust and lithosphere through the process of subduction recycling. The recycling of lower oceanic crust and lithosphere into a host mantle could have resulted in low $\delta^{18}O$ in Pali Aike olivines. Additionally, the oxygen isotopic composition of the mantle reservoir could not have varied according to the relative ages of its components. The oxygen isotopic compositions of subducting hydrothermally altered oceanic crust (±lithosphere) are various and low relative to those of unmodified upper mantle, and these can be used to explain the involvement of subducted and recycled lower oceanic crust in

asthenospheric upwellings by mantle convection.

Therefore, the Pali Aike lavas are located near a destructive plate margin characterized by continuous subduction. The regional tectonic process indicates that slab sinks continuously into the mantle. It is more likely that recycled crustal materials exist in upwelling asthenosphere melt on a small scale. The low oxygen isotopic compositions of Pali Aike olivines with high MgO can be explained by recycling of altered oceanic crust and lithosphere into the mantle source.

Source composition beneath Pali Aike

The chemical characteristics of the Pali Aike lavas are similar to those of HIMU-type OIB (e.g., St. Helena and Antarctica) for trace element and radiogenic (Sr, Nd, and Pb) isotopic compositions (Choo *et al.*, 2012). In particular, the Pb isotopic compositions of Pali Aike lavas are similar to typical HIMU-type OIB and have HIMU affinity with Cenozoic lavas from the Antarctic Peninsula, West Antarctica, and New Zealand (e.g., Panter *et al.*, 2006; Timm *et al.*, 2009, 2010; McCoy-West *et al.*, 2010), previous neighbors in the Gondwana supercontinent (e.g., Rapalini, 2005; Pankhurst *et al.*, 2006). The widespread HIMU mantle source region of the southwestern Pacific extended to the Antarctic Peninsula, West Antarctica, and New Zealand Cenozoic intraplate magmatism. These magmas were derived from lithospheric mantle. The volcanism of the HIMU magmatic megaprovince has been explained by low-degree melting of metasomatized lithospheric mantle with HIMU-like mantle components (Finn *et al.*, 2005; Panter *et al.*, 2006; Sprung *et al.*, 2007) and by removal of metasomatized lithospheric mantle, causing asthenospheric upwelling (Hoernle *et al.*, 2006a, b; Mortimer *et al.*, 2006; Timm *et al.*, 2009). Recently, it has been suggested that the petrogenesis of the HIMU-like signature of Pali Aike lavas may have originated from the sub-continental lithospheric mantle of Gondwana, which had HIMU characteristics at a large scale (Choo *et al.*, 2012). The characteristics of the HIMU-like component for Pali Aike lavas may have been generated by a subduction-related process along the Gondwana margin and by delamination (or detachment) of old subcontinental lithospheric mantle (SCLM) of HIMU-type throughout the Mesozoic. It is proposed that the upper mantle beneath the Pali Aike volcanic field contains a component of HIMU-type with the form of eclogite and/or pyroxenite (Choo *et al.*, 2012).

Recently, the mineral chemistry of olivine phenocrysts has been used to argue that eclogite or pyroxenite is present in OIB-source mantle (Sobolev *et al.*, 2005, 2007). The amount of pyroxenite-derived melt fraction in the parental magma was inferred from olivine composition (Sobolev *et al.*, 2008; Gurenko *et al.*, 2009, 2010). Because olivine is the first mineral phase to precipitate at

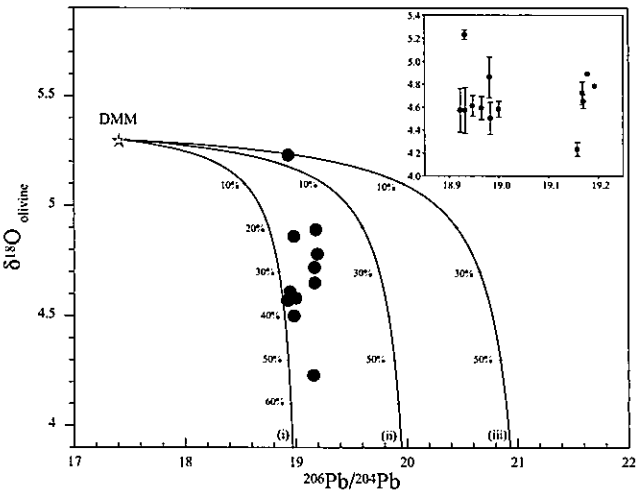

Fig. 8. Plots of whole-rock $^{206}Pb/^{204}Pb$ versus $\delta^{18}O$ in olivine for Pali Aike lavas. The shaded star symbol represents MORB (or the DMM) with olivine $\delta^{18}O$ values of 5.3 ± 0.1‰ (Eiler, 2001). HIMU components are from Timm et al. (2009) and Day et al. (2014). Models (i), (ii), and (iii) show mixing between DMM and HIMU components with $^{206}Pb/^{204}Pb$ of 19, 20, and 21, respectively. Percentages on each curve indicate the proportion of HIMU components within DMM.

low pressure in mantle-derived magmas and forsterite compositions of olivine reconstruct the parental melt composition by the degree of the fractional crystallization, olivine was used as a probe of parental melt composition (Sobolev *et al.*, 2007). As Ni is less and Mn is more compatible in pyroxenite relative to peridotite, the pyroxenite-derived melts were more enriched in Ni and depleted in Mn than the peridotite-derived melts were. Thus, the Ni and Mn contents in olivine can be used to infer the amount of recycled material in the magma source (Sobolev *et al.*, 2005, 2007).

In a similar way, we can calculate the proportion of pyroxenite (X_{px}) in the mantle source beneath Pali Aike using the equation for Ni contents from Sobolev *et al.* (2008):

$$X_{px} = 10.54 \times (Ni \times FeO/MgO) - 0.4368,$$

where X_{px} is the weight fraction of pyroxenite-derived melt. Pure peridotite mantle-derived melts have $X_{px} = 0$, and pyroxenite-derived melts have $X_{px} = 1$. The proportions of calculated pyroxenite-derived melts from the olivine chemistry of Pali Aike lavas are 0.3 to 0.6. HIMU-like Pali Aike lavas require diverse proportions of pyroxenite in their mantle sources. Additionally, the oxygen isotopic compositions of mantle-inherited SCLM with an HIMU-type mantle component of Gondwanaland are observed in HIMU megaprovince Cenozoic alkali basalts

of West Antarctica and New Zealand at a large scale (Nardini *et al.*, 2009; Timm *et al.*, 2009; McCoy-West *et al.*, 2010; Perinelli *et al.*, 2011). The $\delta^{18}O$ values of olivines in HIMU-like Cenozoic alkaline basalts in New Zealand (4.7–5.0‰) and West Antarctica (4.92–5.53‰) and those in wehrlite and clinopyroxenite in mantle xenoliths in Northern Victoria Land (NVL, 5.00–5.72‰) were lower than or nearly equivalent to those of normal-mantle signature (Nardini *et al.*, 2009; Timm *et al.*, 2009; McCoy-West *et al.*, 2010; Perinelli *et al.*, 2011). Cenozoic basalts of the HIMU megaprovince of supercontinental SCLM prior to Gondwana breakup had similar oxygen isotope composition; however, the interpretation for these low $\delta^{18}O$ values was focused on the distinct meaning of crustal contamination by fractional crystallization and the existence of recycled oceanic lithosphere in the source. Alternatively, oxygen isotopic compositions of the magmatic HIMU megaprovince are similar to those of HIMU-type oceanic basalts (4.7–5.56‰; Eiler *et al.*, 1997; Day *et al.*, 2009, 2010; Gurenko *et al.*, 2010).

Similar to these results, Canary Island lavas with HIMU affinity are related to the low $\delta^{18}O$ of olivine and high $^{206}Pb/^{204}Pb$ suggested by Day and colleagues and by Gurenko and colleagues (Day *et al.*, 2009, 2010; Gurenko *et al.*, 2010). To understand the correlation between HIMU affinity and the low oxygen isotopic composition in the Pali Aike lavas, we plot the $\delta^{18}O$ of olivine and $^{206}Pb/^{204}Pb$ of Pali Aike lavas. A weak correlation between the $\delta^{18}O$ value of olivine and $^{206}Pb/^{204}Pb$ of Pali Aike lavas with HIMU-like signature is observed. The radiogenic isotopic composition of Pali Aike lavas falls between end-members HIMU and N-MORB (Choo *et al.*, 2012). In the relationship between the $\delta^{18}O$ of olivines and $^{206}Pb/^{204}Pb$ of whole rock, the composition of the Pali Aike lavas is located along the mixing line between an upper mantle consisting of MORB-like $\delta^{18}O$ with unradiogenic Pb isotopic signatures and a mantle source with lower $\delta^{18}O$ and elevated $^{206}Pb/^{204}Pb$ values (Fig. 8). To assess the proportion of recycled materials and characteristics of mantle reservoirs in Pali Aike, we present a numerical model of two mixing models based on compositions of MORB mantle and pyroxenite dominated by recycled oceanic crust and/or lithosphere (Fig. 8). End-member compositions in the model are based on mantle composition, whose model values were previously published (Day *et al.*, 2010, 2014; Timm *et al.*, 2009). The models mixed with these components show that the Pali Aike lavas lie in the DMM field of and contributed about 20–55% of remaining HIMU material in the form of pyroxenite and/or eclogite. The $^{206}Pb/^{204}Pb$ ratio lower than that of extreme HIMU lavas indicates that heterogeneous lithologies of pyroxenite and/or eclogite can remain in the mantle source within 2 Ga prior to effective mixing with mantle peridotite. The calculation of the mixing of heterogeneous materials in the mantle is consistent with amounts of pyroxenite dominated by recycled oceanic crust from olivine chemistry. The oxygen isotope data for Pali Aike lavas can be reconciled with models for the generation of HIMU-type $^{206}Pb/^{204}Pb$. Reconciling models for the generation of HIMU-type $\delta^{18}O$ with lithological heterogeneity in the mantle supports the aforementioned suggestions (Stern *et al.*, 1990; Choo *et al.*, 2012), and the source of O-Pb isotopic compositions plays an important role in the HIMU-like signature of erupted Pali Aike lavas. The oxygen isotope heterogeneity of Pali Aike olivines gives evidence for mantle sources with recycled oceanic lithosphere and crustal assimilation at shallow levels during eruption.

Conclusions

(1) We present new oxygen isotope compositions of Pali Aike lavas from southern Patagonia. The measured $\delta^{18}O$ compositions of olivine and matrix are 4.23–5.23‰ and 4.64–5.26‰, respectively. The $\delta^{18}O$ values of olivines of the Pali Aike lavas are lower and range more widely than those of MORB mantle peridotites (5.0–5.4‰).

(2) The difference in $\delta^{18}O$ values between olivine and matrix in the Pali Aike lavas is 0.14–0.50. The $\Delta^{18}O_{melt\text{-}ol}$ value of some samples is within equilibrium, but most samples are in disequilibrium at magmatic temperatures. The lower $\delta^{18}O_{melt}$ can be modified by interaction with low $\delta^{18}O$ hydrothermally altered rocks.

(3) The lower oxygen values in low Fo content can be explained by the assimilation at a shallow level. These values lie in the range of a weak negative correlation between $\delta^{18}O$ for olivine and $^{87}Sr/^{86}Sr$ for whole rock, supporting this conclusion.

(4) Oxygen isotopic compositions of Pali Aike olivines with high contents of Fo and MgO have a low and variable range relative to MORB olivine. The oxygen isotope composition of Pali Aike olivines associated with HIMU-OIB can be explained by the contribution of recycled materials such as pyroxenite and/or eclogite in mantle.

(5) The heterogeneity of oxygen isotopic compositions in Pali Aike lavas can be supported by assimilation at a shallow level and the presence of recycled materials of hydrothermally altered oceanic crust in the upper mantle.

Acknowledgments—We are grateful to I. Bindeman and B. Pokrovsky for their constructive reviews that greatly improved the manuscript. This study was supported by KOPRI projects (PM14030) and partly funded by the Polar Academic Program (PAP) from Korea Polar Research Institute. We would like to thank I Ahn, SB Park, JY Joo and SH Han for their assistance with analytical work.

References

Agrinier, P., Hekinian, R., Bideau, D. and Javoy, M. (1995) O and H stable isotope compositions of oceanic crust and upper mantle rocks exposed in the Hess Deep near the Galapagos Triple Junction. *Earth Planet. Sci. Lett.* **136**, 183–196.

Ahn, I., Lee, J. I., Kusakabe, M. and Choi, B.-G. (2012) Oxygen isotope measurements of terrestrial silicates using a CO_2-laser BrF_5 fluorination technique and the slope of terrestrial fractionation line. *Geosci. J.* **16**, 7–16.

Alt, J. C. and Bach, W. (2006) Oxygen isotope composition of a section of lower oceanic crust, ODP Hole 735B. *Geochem. Geophys. Geosyst.* **7**, Q12008.

Arthur, M. A., Anderson, T. F. and Kaplan, I. R. (1983) Stable isotopes in sedimentary geology. *SEPM Short Course* **10**, 432.

Auer, S., Bindeman, I., Wallace, P., Ponomareva, V. and Portnyagin, M. (2009) The origin of hydrous, high-$\delta^{18}O$ voluminous volcanism: diverse oxygen isotope values and high magmatic water contents within the volcanic record of Klyuchevskoy volcano, Kamchatka, Russia. *Contrib. Mineral. Petrol.* **157**, 209–230.

Barker, J. A., Menzies, M. A., Thirlwall, M. F. and MacPherson, C. G. (1997) Petrogenesis of Quaternary intraplate volcanism, Sana'a, Yemen: Implications for plume-lithosphere interaction and polybaric melt hybridization. *J. Petrol.* **38**, 1359–1390.

Barker, J. A., MacPherson, C. G., Menzies, M. A., Thirlwall, M. F., Al-Kadasi, M. and Mattey, D. P. (2000) Resolving crustal and mantle contributions to continental flood volcanism, Yemen contraints from mineral oxygen isotope data. *J. Petrol.* **41**, 1805–1820.

Barnicoat, A. C. and Cartwright, I. (1997) The gabbro-eclogite transformation: an oxygen isotope and petrographic study of west Alpine ophiolites. *J. Metamorphic Geol.* **15**, 93–104.

Bindeman, I. N., Ponomareva, V. V., Bailey, J. C. and Valley, J. W. (2004) Volcanic arc of Kamchatka: a province with high-$\delta^{18}O$ magma sources and large-scale $^{18}O/^{16}O$ depletion of the upper crust. *Geochim. Cosmochim. Acta* **68**, 841–865.

Bindeman, I., Gurenko, A., Sigmarsson, O. and Chaussidon, M. (2008) Oxygen isotope heterogeneity and disequilibria of olivine crystals in large volume Holocene basalts from Iceland: Evidence for magmatic digestion and erosion of Pleistocene hyaloclastites. *Geochim. Cosmochim. Acta* **72**, 4397–4420.

Breitsprecher, K. and Thorkelson, D. J. (2009) Neogene kinematic history of Nazca–Antarctic–Phoenix slab windows beneath Patagonia and the Antarctic Peninsula. *Tectonophysics* **464**, 10–20.

Cande, S. C. and Leslie, R. B. (1986) Late Cenozoic tectonics of the southern Chile trench. *J. Geophys. Res.* **91**(B1), 471–496.

Chiba, H., Chacho, T., Clayton, R. N. and Goldsmith, J. R. (1989) Oxygen isotope fractionations involving diopside, forsterite, magnetite, and calcite: Application to geothermometry. *Geochim. Cosmochim. Acta* **53**, 2985–2995.

Choo, M. K., Lee, M. J., Lee, J. I., Kim, K. H. and Park, K.-H. (2012) Geochemistry and Sr–Nd–Pb isotopic constraints on the petrogenesis of Cenozoic lavas from the Pali Aike and Morro Chico area (52°S), southern Patagonia, South America. *Isl. Arc* **21**, 327–350.

Clayton, R. N. and Mayeda, T. (1983) Oxygen isotopes in eucrites, shergottites, nakhlites, and chassignites. *Earth Planet. Sci. Lett.* **62**, 1–6.

Cocker, J. D., Griffin, B. J. and Muehlenbachs, K. (1982) Oxygen and carbon isotope evidence for seawater-hydrothermal alteration of the Macquarie Island ophiolite. *Earth Planet. Sci. Lett.* **61**, 112–122.

Cole, D. R. and Chakraborty, S. (2001) Rates and mechanism of isotopic exchange. *Stable Isotope Geochemistry* (Valley, J. W. and Cole, D. R., eds.), 83–223, Mineralogical Society of America, Washington, D.C.

Coplen, T. B. (1995) Discontinuance of SMOW and PDB. *Nature* **375**, 285.

Corbella, H. (1999) Dataciones radimetricas en Pali Aike, Patagonia Austral. *Actas, XIV Congreso Geologico Argentino* **II**, 269–272.

Criss, R. E. and Taylor, H. P. (1986) Meteoric-hydrothermal systems. *Rev. Mineral. Geochem.* **16**, 373–424.

D'Orazio, M., Agostini, S., Mazzarini, F., Innocenti, F., Manetti, P., Haller, M. J. and Lahesen, A. (2000) The Pali Aike Volcanic Field, Patagonia: slab-window magmatism near the tip of South America. *Tectonophysics* **321**, 407–427.

D'Orazio, M., Agostini, S., Innocenti, F., Haller, M. J., Manetti, P. and Mazzarini, F. (2001) Slab window-related magmatism from southernmost South America: the Late Miocene mafic volcanics from the Estancia Glencross Area (~52°S, Argentina–Chile). *Lithos* **57**, 67–89.

D'Orazio, M., Innocentia, F., Manettib, P., Hallerc, M. J., Di Vincenzo, G. and Tonarini, S. (2005) The Late Pliocene mafic lavas from the Camusu Aike volcanic field (~50°S, Argentina): Evidence for geochemical variability in slab window magmatism. *J. S. Am. Earth. Sci.* **18**(2), 107–124.

Day, J. M. D., Pearson, G., Macpherson, C. G., Lowry, D. and Carrasedo, J.-C. (2009) Pyroxenite-rich mantle formed by recycled oceanic lithosphere: Oxygen-osmium isotope evidence from Canary Island lavas. *Geology* **37**, 555–558.

Day, J. M. D., Pearson, D. G., MacPherson, C. G., Lowry, D. and Carracedo, J. C. (2010) Evidence for distinct proportions of subducted oceanic crust and lithosphere in HIMU-type mantle beneath El Hierro and La Palma, Canary Islands. *Geochim. Cosmochim. Acta* **74**, 6565–6589.

Day, J. M. D., Peters, B. J. and Janney, P. E. (2014) Oxygen isotope systematics of South African olivine melilitites and implications for HIMU mantle reservoirs. *Lithos* **202–203**, 76–84.

DeMets, C., Gordon, R. G., Angus, D. F. and Stein, S. (1994) Effect of recent revisions to the geomagnetic reversal time scale on estimates of current plate motions. *Geophys. Res. Lett.* **21**, 2191–2194.

Demouchy, S., Jacobsen, S. D., Gaillard, F. and Stern, C. R. (2006) Rapid magma ascent recorded by water diffusion profiles in mantle olivine. *Geology* **34**, 429–432.

Dohmen, R., Chakraborty, S. and Becker, H.-W. (2002) Si and O diffusion in olivine and implications for characterizing

plastic flow in the mantle. *Geophys. Res. Lett.* **29**, 26-1–26-4.

Eiler, J. M. (2001) Oxygen isotope variations of basaltic lavas and upper mantle rocks. *Rev. Mineral. Geochem.* **43**, 319–364.

Eiler, J. M., Valley, J. W. and Stolper, E. M. (1996) Oxygen isotope ratio in olivine from the Hawaii Scientific Drilling Project. *J. Geophys. Res.* **101**, 11807–11813.

Eiler, J. M., Farley, K. A., Valley, J. W., Hauri, E., Craig, H., Hart, S. R. and Stolper, E. M. (1997) Oxygen isotope variations in ocean island basalt phenocrysts. *Geochim. Cosmochim. Acta* **61**, 2281–2293.

Eiler, J. M., Schiano, P., Kitchen, N. and Stopler, E. M. (2000) Oxygen-isotope evidence for recycled crust in the sources of mid-ocean-ridge basalts. *Nature* **403**, 530–534.

Ferrar, E. and Dixon, J. M. (1984) Overriding of the Indian–Antarctic Ridge: Origin of Emerald Basin and migration of late Cenozoic volcanism in Southern New Zealand and Campbell Plateau. *Tectonophysics* **104**, 243–256.

Ferrari, L. (2004) Slab detachment control on mafic volcanic pulse and mantle heterogeneity in central Mexico. *Geology* **32**, 77–80.

Finn, C. A., Mueller, R. D. and Panter, K. S. (2005) A Cenozoic diffuse alkaline magmatic province (DAMP) in the southwest Pacific without rift or plume origin. *Geochem. Geophys. Geosyst.* **6**, Q02005.

Friedman, I. and Gleason, J. D. (1973) A new silicate intercomparison standard for ^{18}O analysis. *Earth Planet. Sci. Lett.* **18**, 124–124.

Garcia, M. O., Ito, E., Eiler, J. M. and Pietruszka, A. J. (1998) Crustal contamination of Kilauea Volcano magmas revealed by oxygen isotope analyses of glass and olivine from Puu Oo Eruption Lavas. *J. Petrol.* **39**, 803–817.

Gorring, M. L. and Kay, S. M. (2001) Mantle processes and sources of Neogene slab window magmas from southern Patagonia, Argentina. *J. Petrol.* **42**, 1067–1094.

Gorring, M. L., Kay, S. M., Zeitler, P. K., Ramos, V. A., Rubiolo, D., Fernandez, M. I. and Panza, J. L. (1997) Neogene Patagonian plateau lavas: Continental magma associated with ridge collision at the Chile Triple Junction. *Tectonics* **16**, 1–17.

Gorring, M. L., Singer, B., Gowers, J. and Kay, S. M. (2003) Plio–Pleistocene basalts from the Meseta del Lago Buenos Aires, Argentina: evidence for asthenosphere-lithosphere interactions during slab window magmatism. *Chem. Geol.* **193**, 215–235.

Gregory, R. T. and Taylor, H. P. (1981) An oxygen isotope profile in a section of Cretaceous oceanic crust, Samail Ophiolite, Oman: Evidence for $\delta^{18}O$ buffering of the oceans by deep (>5 km) seawater-hydrothermal circulation at mid-ocean ridges. *J. Geophys. Res.* **86**, 2737–2755.

Griffin, W. L., O'Reilly, S. Y., Abe, N., Aulbach, S., Davies, R. M., Pearson, N. J., Doyle, B. J. and Kivi, K. (2003) The origin and evolution of Archean lithospheric mantle. *Precambrian Res.* **127**, 19–41.

Gripp, A. E. and Gordon, R. G. (2002) Young tracks of hotspots and current plate velocities. *Geophys. J. Int.* **150**, 321–361.

Gurenko, A. A., Sobolev, A. V., Hoernle, K. A., Hauff, F. and Schminche, H.-U. (2009) Enriched, HIMU-type peridotite and depleted recycled pyroxenite in the Canary plume: A mixed-up mantle. *Earth Planet. Sci. Lett.* **277**, 514–524.

Gurenko, A. A., Hoernle, K. A., Sobolev, A. V., Hauff, F. and Schmincke, H.-U. (2010) Source components of the Gran Canaria (Canary Islands) shield stage magmas: evidence from olivine composition and Sr–Nd–Pb isotopes. *Contrib. Mineral. Petrol.* **159**, 689–702.

Gurenko, A. A., Bindemam, I. and Chaussidon, M. (2011) Oxygen isotope heterogeneity of the mantle beneath the Canary Islands: insights from olivine phenocrysts. *Contrib. Mineral. Petrol.* **162**, 349–363.

Hansteen, T. H. and Troll, V. R. (2003) Oxygen isotope composition of xenoliths from the oceanic crust and volcanic edifice beneath Gran Canaria (Canary Islands): consequences for crustal contamination of ascending magmas. *Chem. Geol.* **193**, 181–193.

Harmon, R. S. and Hoefs, J. (1995) Oxygen isotope heterogeneity of the mantle deduced from global ^{18}O systematics of basalts from different geotectonic settings. *Contrib. Mineral. Petrol.* **120**, 95–114.

Hart, S. R., Blusztajn, J. and Craddock, C. (1997) Hobbs Coast Cenozoic volcanism: implications for the West Antarctic rift system. *Chem. Geol.* **139**, 223–248.

Hart, S. R., Blusztajn, J., Dick, H. J. B., Meyer, P. S. and Muehlenbachs, K. (1999) The fingerprint of seawater circulation in a 500-meter section of ocean crust gabbros. *Geochim. Cosmochim. Acta* **63**, 4059–4080.

Hirschmann, M. M., Kogiso, T., Baker, M. B. and Stolper, E. M. (2003) Alkalic magmas generated by partial melting of garnet pyroxenite. *Geology* **31**, 481–484.

Hoernle, K., White, J. D. L., Bogaard, P. V. D., Hauff, F., Coombs, D. S., Werner, R., Timm, C., Garbe-Schönberg, C.-D., Reay, A. and Cooper, A. F. (2006a) Cenozoic intraplate volcanism on New Zealand: upwelling induced by lithospheric removal. *Earth Planet. Sci. Lett.* **248**, 335–352.

Hoernle, K., White, J. D. L., Bogaard, P. V. D., Hauff, F., Coombs, D. S., Werner, R., Timm, C., Garbe-Schönberg, D., Reay, A. and Cooper, A. F. (2006b) Cenozoic intraplate volcanism on New Zealand: Upwelling induced by lithospheric removal. *Earth Planet. Sci. Lett.* **248**, 350–367.

Hofmann, A. W. and White, W. M. (1982) Mantle plumes from ancient oceanic crust. *Earth Planet. Sci. Lett.* **57**, 421–436.

Hofmann, A. W., Jochum, K. P., Seufert, M. and White, W. M. (1986) Nb and Pb in oceanic basalts: new constraints on mantle evolution. *Earth Planet. Sci. Lett.* **79**, 33–45.

Ito, E. and Clayton, R. N. (1983) Submarine metamorphism of gabbros from the Mid-Cayman rise: An oxygen isotopic study. *Geochim. Cosmochim. Acta* **47**, 535–546.

Ito, E., White, W. M. and Gopel, C. (1987) The O, Sr, Nd and Pb isotope geochemistry of MORB. *Chem. Geol.* **62**, 157–176.

Jabeen, I. and Kusakabe, M. (1997) Determination of $\delta^{17}O$ values of reference water samples VSMOW and SLAP. *Chem. Geol.* **143**, 115–119.

Kempton, P. D., Hawkesworth, C. J. and Fowler, M. (1991) Geochemistry and isotopic composition of gabbros from layer 3 of the Indian ocean crust, Hole 735B. *Proceedings of the Ocean Drilling Program, Scienfitic Results*, **Vol. 118**,

127–143.
Kogiso, T. and Hirschmann, M. M. (2006) Partial melting experiments of bimineralic eclogite and the role of recycled mafic oceanic crust in the genesis of ocean island basalts. *Earth Planet. Sci. Lett.* **249**, 188–199.
Kogiso, T., Hirschmann, M. M. and Frost, D. J. (2003) High-pressure partial melting of garnet pyroxenite: possible mafic lithologies in the source of ocean island basalts. *Earth Planet. Sci. Lett.* **216**, 603–617.
Kusakabe, M. and Matsuhisa, Y. (2008) Oxygen three-isotope ratios of silicate reference materials determined by direct comparision with VSMOW-oxygen. *Geochem. J.* **42**, 309–317.
Kusakabe, M., Maruyama, S., Nakamura, T. and Yada, T. (2004) CO_2 laser-BrF_5 fluorination technique for analysis of oxygen three isotopes of rocks and minerals. *J. Mass Spectrom. Soc. Japan* **52**, 205–212.
Kyser, T. K. (1990) Stable isotopes in the continental lithospheric mantle. *The Continental Lithospheric Mantle* (Menzies, M., ed.), 127–156, Oxford University Press, NY.
Kyser, T. K., O'Neil, J. R. and Carmichael, I. S. E. (1981) Oxygen isotope thermometry of basic lavas and mantle nodules. *Contrib. Mineral. Petrol.* **77**, 11–23.
Lassiter, J. C. and Hauri, E. H. (1998) Osmium-isotope variations in Hawaiian lavas: evidence for recycled oceanic lithosphere in the Hawaiian plume. *Earth Planet. Sci. Lett.* **164**, 483–496.
Lecuyer, C. and Reynard, B. (1996) High-temperature alteration of oceanic gabbros by seawater (Hess Deep, Ocean Drilling Program Leg 147): Evidence from oxygen isotopes and elemental fluxes. *J. Geophys. Res.* **101**, 15883–15897.
Lee, J. I., Hur, S. D., Choe, M. Y., Yoo, C. M. and Nagao, K. (2000) Geochemistry and K–Ar ages of the Pali-Aike Plateau basalts in the southern Patagonia, South America. *J. Geol. Soc. Korea* **36**, 119–136.
Lee, M. J., Lee, J. I., Kwon, S.-T., Choo, M. K., Jeong, K.-S., Cho, J.-H. and Kim, S.-R. (2011) Sr–Nd–Pb isotopic compositions of submarine alkali basalts recovered from the South Korea Plateau, East Sea. *Geosci. J.* **15**(2), 149–160.
Linares, E. and Gonzalez, R. R. (1990) Catalogo de edades radimetricas de la Republica Argentina 1957–1987. *Asociacion Geologica Argentina, Publicaciones Especiales Serie B* **19**, 628.
Martin, E., Bindeman, I. and Grove, T. L. (2011) The origin of high-Mg magmas in Mt Shasta and Medicine Lake volcanoes, Cascade Arc (California): higher and lower than mantle oxygen isotope signatures attributed to current and past subduction. *Contrib. Mineral. Petrol.* **162**, 945–960.
Mattey, D., Lowry, D. and Macpherson, C. (1994) Oxygen isotope composition of mantle peridotite. *Earth Planet. Sci. Lett.* **128**, 231–241.
Mayr, C., Lücke, A., Stichler, W., Trimborn, P., Ercolano, B., Oliva, G., Ohlendorf, C., Soto, J., Fey, M., Haberzettl, T., Janssen, S., Schäbitz, F., Schleser, G. H., Wille, M. and Zolitschka, B. (2007) Precipitation origin and evaporation of lakes in semi-arid Patagonia (Argentina) inferred from stable isotopes ($\delta^{18}O$, $\delta^{2}H$). *J. Hydrol. Hydromech.* **334**, 53–63.
McCoy-West, A. J., Baker, J. A., Faure, K. and Wysoczanski, R. (2010) Petrogenesis and origins of mid-Cretaceous continental intraplate volcanism in Marlborough, New Zealand: Implications for the long-lived HIMU magmatic megaprovince of the SW Pacific. *J. Petrol.* **51**, 2003–2045.
McCulloch, M. T., Gregory, R. T., Wasserburg, G. J. and Taylor, H. P. J. (1981) Sm–Nd, Rb–Sr, and $^{18}O/^{16}O$ isotopic systematics in an oceanic crustal section: Evidence from the Samail ophiolite. *J. Geophys. Res.* **86**, 2721–2735.
Mortimer, N., Hoernle, K., Hauff, F., Palin, J. M., Dunlap, W. J., Werner, R. and Faure, K. (2006) New constraints on the age and evolution of the Wishbone Ridge, southwest Pacific Cretaceous microplates, and Zealandia-West Antarctica breakup. *Geology* **34**(3), 185–188.
Muehlenbachs, K., Furnes, H., Fonneland, H. C. and Hellevang, B. (2004) Ophiolites as faithful records of ancient seawater: the Solund-Stavfjord Ophiolite Complex as a Late Ordovician example. *Ophiolites in Earth History* **218**, 1–14.
Nardini, I., Armienti, P., Ricchi, S., Dallai, L. and Harrison, D. (2009) Sr–Nd–Pb–He–O isotope and geochemical constraints on the genesis of Cenozoic magmas from the West Antarctic rift. *J. Petrol.* **50**, 1359–1375.
Pankhurst, R. J., Leat, P. T., Sruoga, P., Rapela, C. W., Marquez, M., Strorey, B. C. and Riley, T. R. (1998) The Chon Aike Province of Patagonia and related rocks in West Antarctica: A silicic large igneous province. *J. Volcanol. Geotherm. Res.* **81**, 113–136.
Pankhurst, R. J., Papela, C. W., Fannig, C. M. and Márquez, M. (2006) Gondwanide continental collision and the origin of Patagonia. *Earth-Sci. Rev.* **76**, 235–257.
Panter, K. S., Hart, R. S., Kyle, P. R., Blusztain, J. and Wilch, T. (2000) Geochemistry of Late Cenozoic basalts from the Crary Mountains : characterization of mantle sources in Marie Byrd Land, Antarctica. *Chem. Geol.* **165**, 215–241.
Panter, K. S., Blusztain, J., Hart, R. S., Kyle, P. R., Esser, R. and McIntosh, W. C. (2006) The origin of HIMU in the SW Pacific: evidence from intraplate volcanism in southern New Zealand and subantarctic islands. *J. Petrol.* **47**, 1673–1704.
Pardo-Casa, F. and Molnar, P. (1987) Relative motion of the Nazca (Fallaron) and South American plates since Late Cretaceous time. *Tectonics* **6**, 233–248.
Perinelli, C., Armienti, P. and Dallai, L. (2011) Thermal evolution of the lithosphere in a rift environment as inferred from the geochemistry of mantle cumulates, Northern Victoria Land, Antarctica. *J. Petrol.* **52**, 665–690.
Popova, O. P., Jenniskens, P., Emel'yanenko, V., Kartashova, A., Biryukov, E., Khaibrakhmanov, S., Shuvalov, V., Rybnov, Y., Dudorov, A., Grokhovsky, V. I., Badyukov, D. D., Yin, Q.-Z., Gural, P. S., Albers, J., Granvik, M., Evers, L. G., Kuiper, J., Kharlamov, V., Solovyov, A., Rusakov, Y. S., Korotkiy, S., Serdyuk, I., Korochantsev, A. V., Larionov, M. Y., Glazachev, D., Mayer, A. E., Gisler, G., Gladkovsky, S. V., Wimpenny, J., Sanborn, M. E., Yamakawa, A., Verosub, K. L., Rowland, D. J., Roeske, S., Botto, N. W., Friedrich, J. M., Zolensky, M. E., Le, L., Ross, D., Ziegler, K., Nakamura, T., Ahn, I., Lee, J. I., Zhou, Q., Li, X.-H., Li, Q.-L., Liu, Y., Tang, G.-Q., Hiroi, T., Sears, D., Weinstein, I. A., Vokhmintsev, A. S., Ishchenko, A. V., Schmitt-Kopplin, P., Hertkorn, N., Nagao, K., Haba, M. K.,

Komatsu, M. and Mikouchi, T. (2013) Chelyabinsk airburst, damage assessment, meteorite recovery, and characterization. *Science* **342**, 1069–1073.

Rapalini, A. E. (2005) The accretionary history of southern South America from the latest Proterozoic to the late Paleozoic: some palaeomagnetic constraints. *Geol. Soc. London Special Publ.* **246**, 305–328.

Ross, P.-S., Delpit, S., Haller, M. J., Németh, K. and Corvella, H. (2011) Influence of the substrate on maar-diatreme volcanoes—An example of a mixed setting from the Pali Aike volcanic field, Argentina. *J. Volcanol. Geotherm. Res.* **201**, 253–271.

Rumble, D. I., Farquhar, J., Young, E. D. and Christensen, C. P. (1997) In situ oxygen isotope analysis with an excimer laser using F_2 and BrF_5 reagents and O_2 gas as analyte. *Geochim. Cosmochim. Acta* **61**, 4229–4234.

Schaefer, B. F., Turner, S., Parkinson, I., Rogers, N. and Hawkesworth, C. (2002) Evidence for recycled Archaean oceanic mantle lithosphere in the Azores plume. *Nature* **420**, 304–307.

Schulte, R. F., Schilling, M., Anma, R., Farquhar, J., Horan, M. F., Komiya, T., Piccoli, P. M., Pitcher, L. and Walker, R. (2009) Chemical and chronologic complexity in the convecting upper mantle: Evidence from the Taitao ophiolite, southern Chile. *Geochim. Cosmochim. Acta* **73**, 5793–5819.

Sheppard, S. M. F. and Taylor, H. P. (1974) Hydrogen and oxygen isotope evidence for the origins of water in the Boulder Batholith and the Butte Ore Deposits, Montana. *Econ. Geol.* **69**, 926–946.

Singer, B. S., Ton-That, T., Vincze, T., Rabassa, J., Roig, C. and Brunstad, K. (1997) Timescale of late Cenozoic climate change in the southern hemisphere from $^{40}Ar/^{39}Ar$ dating of Patagonia lavas. *Terra Abstr., Eur. Union Geosci.* **9**, 65–66.

Skewes, M. A. and Stern, C. R. (1979) Petrology and geochemistry of alkali basalts and ultramafic inclusions from the palei-aike volcanic field in Southern Chile and the origin of the patagonian plateau lavas. *J. Volcanol. Geotherm. Res.* **6**, 3–25.

Sobolev, A. V., Hofmann, A. W., Sobolev, S. V. and Nikogosian, I. K. (2005) An olivine-free mantle source of Hawaiian shield basalts. *Nature* **434**, 590–597.

Sobolev, A. V., Hofmann, A. W., Kuzmin, D. V., Yaxley, G. M., Arndt, N. T., Chung, S.-L., Danyushevsky, L. V., Elliott, T., Frey, F. A., Garcia, M. O., Gurenko, A. A., Kamenetsky, V. S., Kerr, A. C., Krivolutskaya, N. A., Matvienkov, V., Nikogosian, I. K., Rocholl, A., Sigurdsson, I. A., Sushchevskaya, N. and Teklay, M. (2007) The amount of recycled crust in sources of mantle-derived melts. *Science* **316**, 412–417.

Sobolev, A. V., Hofmann, A. W., Brugmann, G., Batanova, V. G. and Kuzmin, D. V. (2008) A quantitative link between recycling and osmium isotope. *Science* **321**, 536.

Sprung, P., Schuth, S., Münker, C. and Hoke, L. (2007) Intraplate volcanism in New Zealand: the role of fossil plume material and variable lithospheric properties. *Contrib. Mineral. Petrol.* **153**, 669–687.

Stakes, D. (1991) Oxygen and hydrogen isotope compositions of oceanic plutonic rocks: High-temperature deformation and metamorphism of oceanic layer 3. *Stable Isotope Geochem.* **3**, 77–90.

Staudigel, H., Davies, G. R., Hart, S. R., Marchant, K. M. and Smith, B. M. (1995) Large scale isotopic Sr, Nd and O isotopic anatomy of altered oceanic crust: DSDP/ODP sites 417/418. *Earth Planet. Sci. Lett.* **130**, 169–185.

Stern, C. R., Frey, F. A., Futa, K., Zartman, R. E., Peng, Z. and Kyser, T. K. (1990) Trace-element and Sr, Nd, Pb and O isotopic composition of Pliocene and Quaternary alkali basalt of the Patagonian Plateau lavas of southernmost South America. *Contrib. Mineral. Petrol.* **104**, 294–308.

Stern, C. R., Kilian, R., Olker, B., Hauri, E. H. and Kyser, T. K. (1999) Evidence from mantle xenoliths for relatively this (<100 km) continental lithosphere beleow the Phanerozoic crust of southernmost South America. *Lithos* **48**, 217–235.

Taylor, H. P., Jr. (1968) The oxygen isotope geochemistry of igneous rocks. *Contrib. Mineral. Petrol.* **19**, 1–71.

Taylor, H. P., Jr. and Epstein, S. (1962) Relationship between O^{18}/O^{16} ratios in coexisting minerals of igneous and metamorphic rocks. Part 1: Principles and experimental results. *Amer. Geol. Soc. Bull.* **73**, 461–480.

Thirlwall, M. F., Gee, M. A. M., Lowry, D., Mattey, D. P., Murton, B. J. and Taylor, R. N. (2006) Low $\delta^{18}O$ in the Icelandic mantle and its origins: Evidence from Reykjanes Ridge and Icelandic lavas. *Geochim. Cosmochim. Acta* **70**, 993–1019.

Timm, C., Hoernle, K., Bogaard, P. V. D., Bindemann, I. and Weaver, S. D. (2009) Geochemical evolution of intraplate volcanism at Banks Peninsula, New Zealand: interaction between asthenospheric and lithospheric melts. *J. Petrol.* **50**(6), 989–1023.

Timm, C., Hoernle, K., Werner, R., Hauff, F., Bogaard, P. V. D., White, J., Mortimer, N. and Garbe-Schönberg, D. (2010) Temporal and geochemical evolution of the Cenozoic intraplate volcanism of Zealandia. *Earth-Sci. Rev.* **98**, 38–64.

Tollan, P. M. E., Bindeman, I. and Blundy, J. D. (2012) Cumulate xenoliths from St. Vincent, Lesser Antilles Island Arc: a window into upper crustal differentiation of mantle-derived basalts. *Contrib. Mineral. Petrol.* **163**, 189–208.

Turner, S., Tonarini, S., Bindeman, I., Leeman, W. P. and Schaefer, B. F. (2007) Boron and oxygen isotope evidence for recycling of subducted components over the past 2.5 Gyr. *Nature* **447**, 702–705.

Valley, J. W., Kitchen, N., Kohn, M. J., Niendorf, C. R. and Spicuzza, M. J. (1995) UWG-2, a garnet standard for oxygen isotope ratios: Strategies for high procision and accuracy with laser heating. *Geochim. Cosmochim. Acta* **59**, 5223–5231.

Wang, Z., Kitchen, N. E. and Eiler, J. M. (2003) Oxygen isotope geochemistry of the second HSDP core. *Geochem. Geophys. Geosyst.* **4**.

Warren, P. H., Rubin, A. E., Isa, J., Brittenham, S., Ahn, I. and Choi, B.-G. (2013) Northwest Africa 6693: A new type of FeO-rich, low-$\Delta^{17}O$, poikilitic cumulate achondrite. *Geochim. Cosmochim. Acta* **107**, 135–154.

Weaver, S. D., Storey, B. C., Pankhurst, R. J., Mukasa, S. B., DiVenere, V. J. and Bradshaw, J. D. (1994) Antarctica–New Zealand rifting and Marie Byrd Land lithospheric

magmatism linked to ridge subduction and mantle plume activity. *Geology* **22**, 811–814.
Widom, E. and Farquhar, J. (2003) Oxygen isotope signatures in olivines from Sao Miguel (Azores) basalts: implications for crustal and mantle processes. *Chem. Geol.* **193**, 237–255.
Workman, R. K., Eiler, J. M., Hart, S. R. and Jackson, M. G. (2008) Oxygen isotopes in Samoan lavas: Confirmation of continent recycling. *Geology* **36**, 551–554.
Yurimoto, H., Morioka, M. and Nagasawa, H. (1992) Oxygen self-diffusion along high diffusivity paths in forsterite. *Geochem. J.* **26**, 181–188.
Zindler, A. and Hart, S. R. (1986) Chemical geodynamics. Annual review. *Earth Planet. Sci. Lett.* **14**, 493–571.

Supplementary Materials

URL (http://www.terrapub.co.jp/journals/GJ/archives/data/49/MS333.pdf)
Table S1